Investigating the Modulation of Monometallic Single-Molecule Magnets Through Peripheral Ligand Modifications

Nastaran Ghorbanian Farahabadi

Thesis submitted to the

Faculty of Graduate and Postdoctoral Studies

In partial fulfillment of the requirements for

The M.Sc. degree in Chemistry

Ottawa-Carleton Chemistry Institute

University of Ottawa

Supervisor: *Professor Darrin Richeson*

I would like to dedicate this thesis to my parents for their love and support.

Acknowledgement

First and foremost, I wish to thank my supervisor, Dr. Darrin Richeson, who guided me throughout my scientific research and acted as a support system for me while studying far from home. His daily presence in the lab and his advice provided me with insight at times when my results were not as expected and when experiencing difficulties in my research.

Furthermore, I would like to thank the Richeson group, who have made the lab an enjoyable place to work. I would like to thank my great friend, Sarah, who helped me so much, as well as Titel from whom I learned most of my laboratory techniques, along with Phil, Sheila and Ahmed for being amazing lab mates. In addition, I would like to thank Dr. Ilia Korobkov, our crystallographer. The results of my research would not be the same without his help and enthusiasm.

I would like to thank my parents who have been incredibly supportive throughout this entire process. Without their constant love and encouragement I would not have completed this thesis. I would also like to thank my sister, Sara, for all her love and advice, as well as my brother, Masoud, for his continuous support and with whom I have shared so many fantastic moments. I would like to thank my aunt, Nasrin, who has acted as a support system for me in Ottawa.

I want to give special thanks to my best friend, Saba. His encouragement has been very important to me as he has always celebrated with me in the good times and supported me in the hard times. It is with the help and support of all these important individuals that I have been able to achieve the results that I have in this thesis and I thank and acknowledge them immensely.

Abstract

This thesis focuses on the synthesis of mononuclear Co and Fe complexes of defined geometry. The goal is to explore the effects of metal coordination geometry on single molecule-magnets (SMM) through peripheral ligand modification with the bis(imino)pyridine ligand. **Chapter 1** presents fundamental concepts that are used in the molecular magnetism and single molecule magnets. **Chapter 2** describes a history and synthesis of the bis(imino)pyridine ligand. **Chapter 3** discusses the synthesis of Cobalt (II) bis(imino)pyridine complexes with varied sterics, their characterization, structural analysis and magnetic properties. **Chapter 4** presents the synthesis of Iron (II) bis(imino)pyridine complexes with varied sterics, their characterization, structural analysis and magnetic properties. **Chapter 5** provides a summary of the work presented in this thesis.

Table of Contents

List of Figures

List of Tables

Chapter 1

Introduction to Magnetic Properties of Complexes and Single Molecule Magnets (SMMs).

Magnetism has been known by humans for thousands of years. An example is provided by Lodestone, a naturally occurring magnetized mineral that will attract iron and was probably the first magnetic material know to ancient man. The vast majority of magnetic materials were structurally based on metallic and ionic lattices. At the end of twentieth century, a new research field, molecular magnetism, was opened when the first examples of magnets based on organic compounds were observed.[1]

Molecular magnetism is a particular subset of magnetic materials that focuses on the magnetic properties of isolated molecules or assemblies of molecules. These systems contain one or more magnetic centers.[2] Molecular magnetism combines efforts in synthetic chemistry with ideas from theoretical chemistry, and a main challenge in molecular magnetism is to design and synthesize molecular systems that display predictable magnetic properties. To reach this target, several kinds of inorganic compounds, organic radicals and polymers containing bridging groups were synthesized.

One of the most interesting areas in molecular magnetism is a class of molecules known as a single-molecule magnets. These molecules undergo a slow magnetic relaxation and display magnetic hysteresis that is molecular in origin. This new and exciting

[1] Gatteschi, D.; Sessoli, R.; Villain, J.; In *Molecular Nanomagnets.*. Oxford University Press, Inc.; NewYork, **2006**.

[2] O. Kahn, In *Molecular Magnetism*, Wiley-VCH: Weinheim, Germany, **1993**.

observation contrasts with classical bulk magnetic materials. Single-molecule magnets can be viewed to behave as tiny magnets that show a slow magnetic relaxation behavior at low temperature.

This thesis is particularly devoted to the synthesis and characterization of cobalt and iron complexes that are targeted to behave as single-molecule magnets. In order to put this effort into context it is first necessary to explain some generalities concerning magnetism, magnetic susceptibility and some fundamental equations that are used in this field.

[1.1] Magnetic Susceptibility

Put in its simplest terms, the magnetization (M) of the material that is induced by a given applied field (H_o), is related to applied field (H_o) by the following Equation 1.1 where χ is the magnetic susceptibility.[3]

$$\chi = M / H_o \qquad \textbf{Equation 1.1}$$

[1.2] Diamagnetic and Paramagnetic

Diamagnetism is a property of all matter that arises from the fact that most of the electrons in matter are paired and that the interaction of electron pairs with an applied field (H_o) generates a field opposing the applied field. These materials are repelled by the applied field (H_o). With increasing the applied field the energy of the system (E) increases, hence the

[3] Murugesu, M.; *Special Topics in Inorganic Chemistry: Molecular Magnetism*. **2013**. Department of Chemistry; University of Ottawa.

sign of the magnetization (M) which is induced by the applied field (H_o), and magnetic susceptibility (χ^D) for diamagnetic materials are negative (Equation 1.2).[4]

$$M = - \sigma E / \sigma H_o \qquad \textbf{Equation 1.2}$$

Paramagnetism arises in the presence of unpaired electrons. In contrast with diamagnetic materials, paramagnetic materials are attracted by applied field. Importantly, these materials will have a diamagnetic component as well, due to any paired electrons. The sign of the magnetization (M), and therefore magnetic susceptibility (χ^P) for paramagnetic materials are positive. The observed magnetic susceptibility (χ^O) is given by Equation 1.3 and depends on whether diamagnetism or paramagnetism dominates in the system.

$$\chi^O = \chi^D + \chi^P \qquad \textbf{Equation 1.3}$$

[1.3] The Curie Law and Magnetic Interactions

It was discovered experimentally by Pierre Curie that for most paramagnetic materials with isolated magnetic sites, the magnetic susceptibility is inversely proportional to temperature (Equation 1.4).

$$\chi = C/T \qquad \textbf{Equation 1.4}$$

For instance, in the absence of applied magnetic field the two levels $m_s = \pm 1/2$ are degenerate. When the field is applied, the two levels split (Figure 1.1), the energy of each

[4] Morgenstern-Badarau, I.; Cocco, D.; Desideri, A.; Rotilio, G.; Jordanov, J.; Dupre, N. *J. Am. Chem. Soc.* **1998**, *108*, 300.

level (E_n) is given by Equation 1.5, therefore the energy difference between two levels is $\Delta E = gBH_o$ for $m_s = \pm 1/2$, and the magnetization (M_n) of a molecule in a given m_s state is given by Equation 1.6. [5-7]

$$E_n = m_s g B H_o \qquad \textbf{Equation 1.5}$$

$$M_n = - \sigma E / \sigma H_o = - m_s g B \qquad \textbf{Equation 1.6}$$

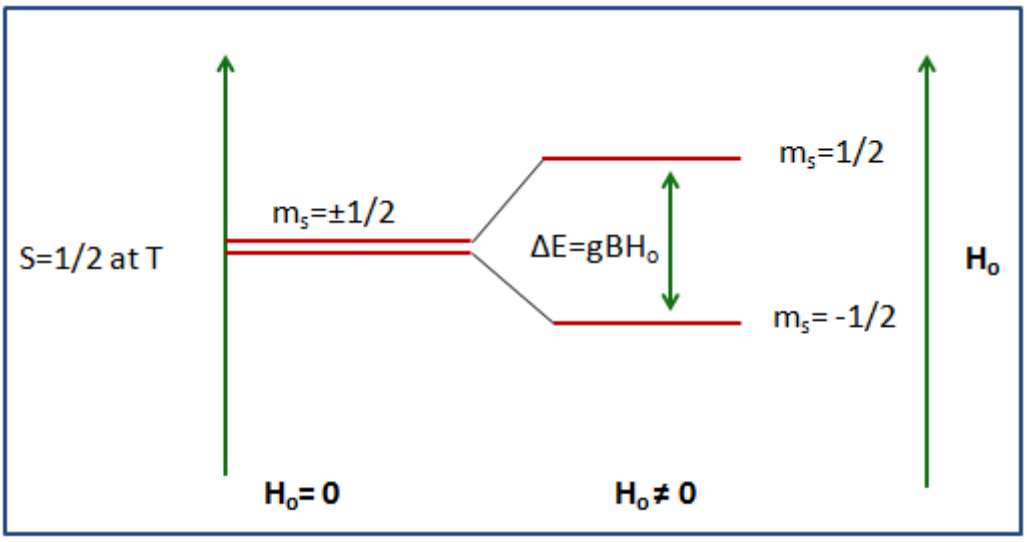

Figure 1.1: Splitting of m_s states in the presence of an applied field (H) for an isolated S = 1/2 spin.

The total magnetization (M) of the sample is the summation of the individual magnetization in direction of applied field weighted by their Boltzmann`s population. The total magnetization and total magnet susceptibility for any S value (S = spin ground state) were shown by Equation 1.7 and 1.8.

---

[5] Bain, G. A.; Berry, J. F.; *J. Chem. Ed*. **2008**, *85*, 532.

[6] Drago, R. S. *Physical Methods in Chemistry*. **1992**, W. B. Saunders Company: Philadelphia.

[7] Carlin, R. L. *Magnetochemistry*. **1986**. Springer-Verlag: Berlin.

$M = Ng^2B^2Ho/3kT\ (S)\ (S+1)$ **Equation1.7**

$\chi T = g^2/8\ (S)\ (S+1)$ **Equation1.8**

For a simple isolated paramagnetic substance, the plot of χT versus T is a straight line parallel to the x-axis at a constant value $[g^2/8(S)(S+1)]$, showing the temperature independence of the magnetic moment (Figure 1.2).

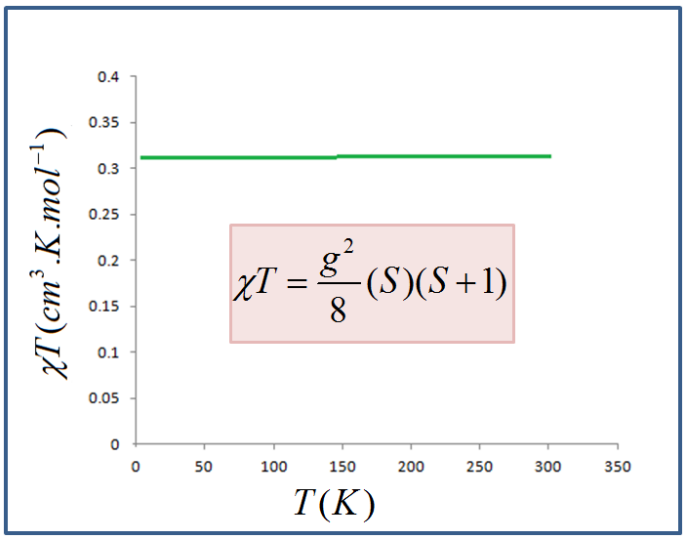

Figure 1.2: χT vs. T plot showing the proportional relationship between magnetic susceptibility and temperature.

The Curie law is valid in the case of an isolated magnetic spin. When there are magnetic interactions between the spin carriers, this law cannot be applied for magnetic behavior.

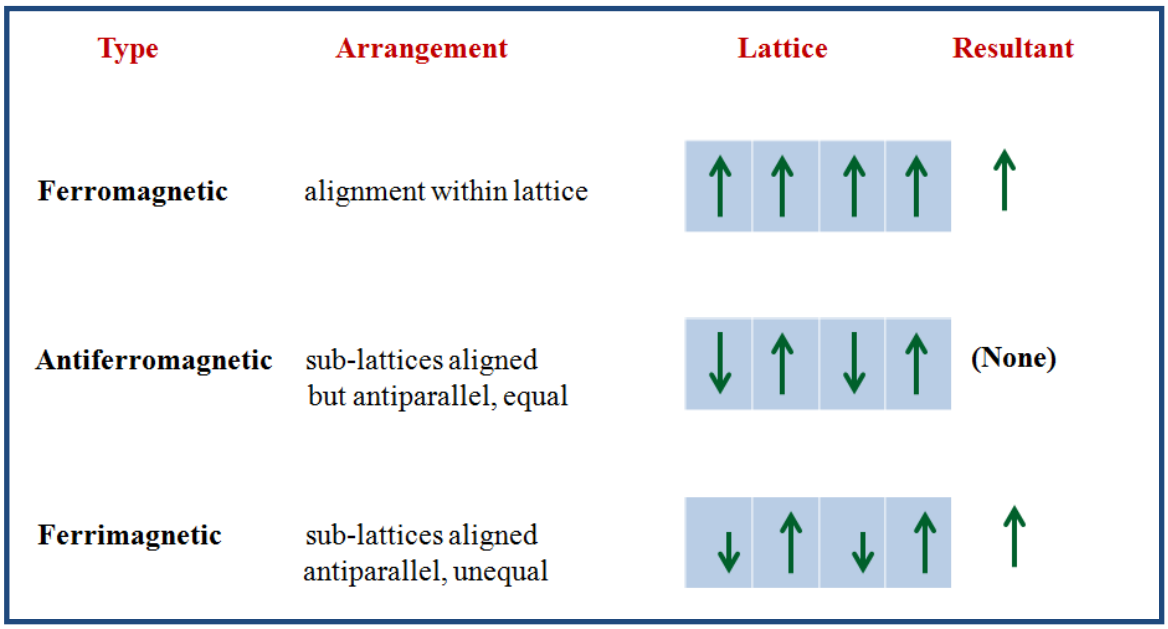

Figure 1.3: The different types of magnetic interactions[8]

When paramagnetic centers interact with each other they can be classified into three different types which are schematically shown in Figure 1.3. The first kind of magnetic interaction is known as ferromagnetic interaction. In this interaction, the individual magnetic spins tend to align with each other and in the direction of an applied magnetic field. In the absence of an applied magnetic field, the spontaneous, preferred alignment means that ferromagnetic materials exhibit magnetization. A second type of magnetic interaction is antiferromagnetic interaction, in this case the magnetic spins display a preference to align in opposing directions and thereby the spins cancel each other. A third type of interaction, which is similar to antiferromagnetic, is known as ferrimagnetic interaction. In ferrimagnetic substances, the spins prefer to be aligned in opposition but the opposing moments are unequal (Figure 1.4).

[8] Image retrieved from http://gravmag.ou.edu/mag_rock/mag_rock.html

The Curie Law can be modified to reflect that there are magnetic interactions between the spin carries to give the Curie-Weiss Law. The magnetic susceptibility is then defined by Equation 1.9, where C is the Curie constant and θ is the Weiss constant.

$\chi = C / T - \theta$ **Equation 1.9**

The decrease of the χT versus T, on cooling is indicative of the presence of antiferromagnetic interaction, where the sign of Weiss constant (θ) is negative and the increase of the χT versus T, on cooling is indicative of the presence of ferromagnetic interaction, where the sign of Weiss constant (θ) is positive (Figure 1.3).

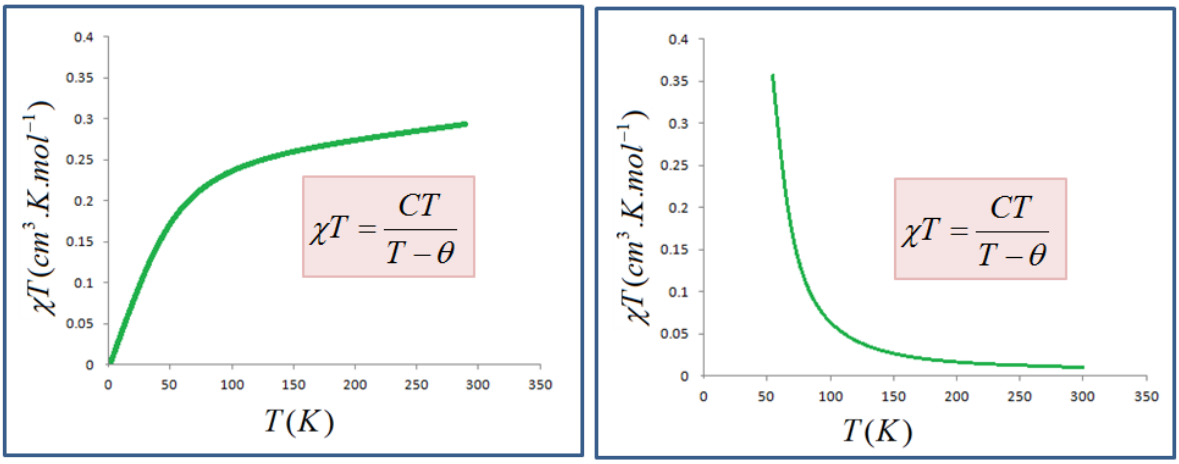

Figure 1.4: χT vs. T plots showing an antiferromagnetic interaction (left) and a ferromagnetic interaction (right).

[1.4] Magnetic Anisotropy

Magnetic anisotropy is a dependence of a materials magnetization on the direction. A simple paramagnetic material is magnetically isotropic and, in the absence of a magnetic field, there is no preferential orientation of the moment. In contrast, a magnetically anisotropic material will align its moment along a specific axis. This axis of spontaneous magnetization is called an "easy" axis and in the absence of a magnetic field the two opposite directions along an easy axis are usually equivalent. Magnetic anisotropy originates from zero-field splitting (ZFS). Zero-field splitting is the removal of the spin degeneracy when $S > 1/2$ in the absence of magnetic applied field.

Coupling of the ground state with excited states via spin–orbit coupling causes zero-field splitting. In most cases, spin–orbit coupling occurs in conjunction with the effects of a structural distortion, for example, away from O_h symmetry.[2] The effect of ZFS on an $S = 3/2$ state is shown in Figure 1.5.[7] When the external magnetic field is applied, the degeneracy of the M_S levels can be removed even in the absence of zero-field splitting (the first order Zeeman effect). When the crystal field is axial, before the external magnetic field is applied, the degeneracy is resolved partially, and the $M_S = \pm 1/2$ levels are separated from the $M_S = \pm 3/2$ levels by $2D$ (D is the axial ZFS parameter).

The metal ion and its coordination geometry can affect on the size of the D parameter.[9] For example, Cr(III) with octahedral geometry and Co(II) with tetrahedral geometry have the same spin ground state $S = 3/2$, but spin-orbit coupling constant for Cr(III) is small and thereby the D values are also small. On the other hand, Co(II) has a larger spin-orbit coupling constant and hence has a larger D parameter.

[9] R. Boca. *Coord. Chem. Rev*. **2004**, *248*, 757.

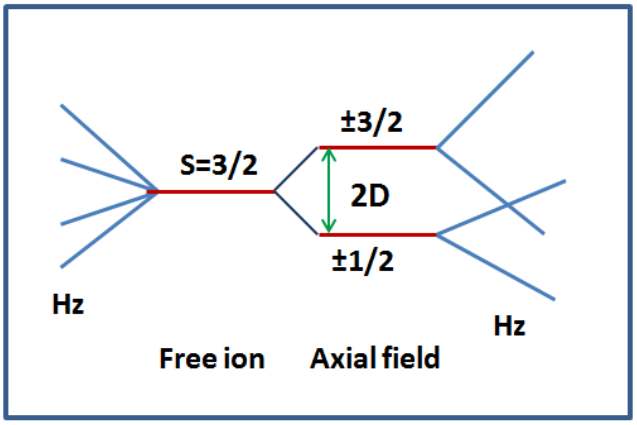

Figure 1.5: Zeeman splitting of an $S = 3/2$ state in the absence (left) and presence (right) of an axial zero-field splitting.

Having a ZFS is important in the preparation of materials designed to show single-molecule magnet properties, as it causes a magnetic anisotropy.[1,10]

[1.5] Single-Molecule Magnets (SMMs)

Single-Molecule Magnets, SMMs, are a class of compounds that retain a magnetic moment (M) after removing an applied magnetic field (H_o). The barrier to magnetic relaxation originates from the negative molecular magnetic anisotropy (D) on nonzero spin ground state (S). This barrier (U) is defined as $U = S^2 |D|$ for integer spin values and (S^2 - 1/4)$|D|$ for half integer spins.

Having a nonzero spin ground state is necessary in the preparation of materials designed to exhibit SMMs behavior. The use of materials containing highly anisotropic metal center has provided another approach to the design SMMs.

[10] Cornia. A; Gatteschi. D; Sessoli. R. *Coord. Chem. Rev.* **2001**, *573,* 219.

$[Mn_{12}O_{12}(CH_3COO)_{16}(H_2O)_4].2CH_3COOH\cdot 4H_2O$ was the first SMM to be observed by Lis in 1980,[11,12] and the term single-molecule magnet was used by Hendrickson in 1996.[13] Molecules containing transition metal, lanthanide or actinide have been shown to exhibit slow magnetic relaxation at low temperature.[14-24] The barrier to magnetic relaxation is proportional to S^2 and most known SMMs compounds are polynuclear complexes with having a high total spin ground state. The best SMM $[Mn_6O_2(Etsao)_6(O_2CPh)_2(EtOH)_6]$ has an $S = 12$ ground state and an energy barrier to magnetization reversal of 86 K ($T_B \approx 4.5$ K).[25] Mononuclear complexes with a low total spin ground state have been shown to exhibit

---

[11] Caneschi, A.; Gatteschi, D.; Sessoli, R.; Barra, A. L.; Brunel, L. C.; Guillot, M. *J. Am. Chem. Soc.* **1991**, *113*, 5873.

[12] Lis, T.; *Acta Cryst. B.* **1980**, *36*, 2042.

[13] Aubin, S. M. J.; Wemple, M. W.; Adams, D. M.; Tsai, H. L.; Christou, G.; Hendrickson, D. N.; *J. Am. Chem. Soc.* **1996**, *118*, 7746.

[14] Zhang, Y-Z.; Wernsdorfer, W.; Pan, F.; Wanga Z-M.; Gao, S. *Chem. Commun*. **2006**, 3302

[15] Jia, Q-X.; Tian, H.; Zhang, J-Y.; Gao, E-Q.; *Chem. Eur. J.* **2011**, *17*, 1040.

[16] Tang, J.; Hewitt, I.; Madhu, N. T.; Chastanet, G.; Wernsdorfer, W.; Anson, C. E.; Benelli, C.; Sessoli, R.; Powell, A. K. *Angew. Chem. Int. Ed.* **2006**, *45*, 1729

[17] Ishikawa, N.; Sugita, M.; Wernsdorfer, W. *J. Am. Chem. Soc.***2005**, *127*, 3650.

[18] Jiang, S.-D.; Wang, B.-W.; Sun, H.-L.; Wang, Z.-M.; Gao, S. *J. Am. Chem. Soc*. **2011**, *133*, 4730.

[19] Li, D. P.; Wang, T. W.; Li, C. H.; Liu, D. S.; Li, Y. Z.; You, X. Z. *Chem. Commun*. **2010**, *46*, 2929.

[20] AlDamen, M. A.; Clemente-Juan, J. M.; Coronado, E.; Marti-Gastaldo, C.; Gaita-Arino, A. *J. Am. Chem. Soc*. **2008**, *130*, 8874.

[21] Rinehart, J. D.; Long, J. R. *J. Am .Chem. Soc*. **2009**, *131*, 12558.

[22] Jiang, S. D.; Wang, B. W.; Su, G.; Wang, Z. M.; Gao, S. *Angew. Chem.,Int. Ed*. **2010**, *49*, 7448.

[23] Magnani, N.; Apostolidis, C.; Morgenstern, A.; Colineau, E.; Griveau, J.-C.; Bolvin, H.; Walter, O.; Caciuffo, R. *Angew. Chem*. **2011**, *50*, 1696.

[24] Rinehart, J. D.; Meihaus, K. R.; Long, J. R. *J. Am. Chem. Soc*. **2010**, *132*, 7572

[25] Milios, C. J.; Vinslava, A.; Wernsdorfer, W.; Moggach, S.; Parsons, S.; Perlepes, S. P.; Christou, G.; Brechin, E. K.; *J. Am. Chem. Soc.* **2007**, *129*, 2754.

slow magnetic relaxation at low temperatures. This SMMs behavior is attributed to the high magnetic anisotropy which is arises due to a high degree of spin-orbit coupling observed in d-block and f-block elements.

Recently SMM behavior have been demonstrated by Chang, Long and co-workers for mononuclear Fe(II) complexes. In these mononuclear SMMs, the highly anisotropic ground state is attributed to the strong spin-orbit coupling.

Inspired by this achievement, we looked at the inherently high magnetic anisotropy elements, from which we targeted a family of five-coordinate Co(II) and Fe(II) compounds.

[1.6] Pentacoordinated Geometry

Valence shell electron pair repulsion (VSEPR) theory can be used to predict the geometry of molecules based on electron-pair electrostatic repulsion.[26] The electron pairs in the valence shell of the central atom repel each other, thereby they arrange themselves to minimize these electrostatic repulsions. Electron pairs, in 2, 3, 4, and 6 coordinate geometries, lie on the surface of the central atom and form a regular polyhedron with all of the angles equivalent and all of the sides of the polygon as equal triangles. But 5 electron pairs around the central atom are unable to form a regular polyhedron with five vertices. Euler mathematically demonstrated that there are five regular platonic solids, (tetrahedron, cube, octahedron, dodecahedron, and icosahedron).[27]-[29] Generally, coordination number 5 is less common than complexes with coordination number 4 and 6. In most cases, the

[26]Jolly, W. L.; *Modern Inorganic Chemistry*, McGraw-Hill,

[27] Coxeter. H.S. M. **1973**. Regular Polytopes (3rd ed.). New York: Dover Publications.

[28] Coxeter, H. S. M. in *Regular Polytopes*, 2nd ed., Macmillan, New York, **1963**.

[29] Hilbert, D.; Cohn-Vossen, S.E. *Geometry and the imagination*, Chelsea .**1952**. p. 9.

complexes with coordination number 5 can lose a ligand and become 4 coordinate or associate, for example with itself to dimerize and become 6 coordinate.

The typical geometries for coordination number 5 are trigonal bipyramidal (tbp) and square-pyramidal (sp). Main group elements tend to prefer to be trigonal bipyramidal. For transition metals both geometries can be seen. There is little energy difference between the two arrangements of ligands. In fact, for the same molecule, both geometries can sometimes be seen. For example, the compound $[Ni(CN)_5]^{3-}$ adopts both geometries and they may easily interconvert in solution.[30-32] This feature suggests a stereochemical nonrigidity for the complexes with coordination number 5.

In a true trigonal bipyramidal (tbp) complex, all of the ligands are identical. In these structures, the point group is D_{3h}. The tbp geometry has two ligand environments; two are axial and three are equatorial positions. The dynamism of tbp is also well-known. For example, the two positions for the ligands in $Fe(CO)_5$ can interchange, axial and equatorial ligands exchange positions with the transition state being the square pyramidal structure[33] This process is called pseudorotation or Berry pseudorotation.[34] As a result, $Fe(CO)_5$ gives only one ^{13}C NMR signal for the resonance of the carbonyl-carbon atoms. The NMR only sees the average structure, because the exchange (pseudorotation) is faster than the NMR timescale. The rate of the pseudorotation can be changed by reducing the

[30] Aristides, T.; Raymond, K. N.; Spiro, T. G. *Inorg.chem.* **1970**, *9*, 2415.

[31] Raymond, K. N.; Corfield, P.W.R.; Ibers. *J. A. Inorg.* **1968**, *7*, 1362.

[32] Raymond, K. N.; Basolo, F. *Inorg.Chem.* **1966**, *5*, 949.

[33] Langer, C. *J. Chem. Soc.,* Trans. **1891**, *59*, 1090.

[34] Cass, M. E.; Hii, K. K.; Rzepa, H. S. *J. Chem. E*, **2005**.

temperature of the measurement, altering the ligand with more sterically bulky ligand, or using a shorter timescale measurement method, like IR spectroscopy.

Similarly to tbp, the square pyramidal (sp) structure has two different positions for the groups; one axial and four basal. Interestingly, a sp structure is preferred when one of the metal-ligand bonds is a multiple bond. Since the sp geometry has non-axial symmetry, a distorted complex can be formed by shifting the central atom along to the molecular axis. That means that the metal can be on the basal plane or a little above it. Again, to be a pure sp geometry, the five ligands should be identical. Since in the majority of complexes the ligands are not identical, the geometry is often not ideal. Furthermore, packing effects in the solid and distortions due to non-bonding orbital effects can be another reason for distortion in geometry.[35]

In 1984, Verschoor suggested a simple calculation to classify molecular geometries as more like tbp or sp.[36] The value τ (Tau) has been used in this calculation to determine how closely a distorted complex approximates either a tbp or sp geometry.[37] Tau, τ, is defined as $(\alpha - \beta)/60$. In this formula, α and β being the largest ligand−metal−ligand angles. In the case of perfectly square pyramidal geometry, since the largest angles are equal to 180° ($\alpha = \beta =$ 180°), τ would be 0.[38] For an ideal trigonal bipyramidal geometry, α becomes 120° and the

---

[35] Kipof. P "Coordination Number 5", (December 2005) Retrieved from: http://www.d.umn.edu/~pkiprof/ChemWebV2/Coordination/CN5.html

[36] Addison, A. W.; Rao, T. N.; Reedijk, J.; van Rijn, J.; Verschoor, G. C. *J. Chem. Soc. Dalton Trans.* **1984**, 1349.

[37] Muetterties, E. L.; Guggenberger. E. J. *J. Am. Chem. Soc.* **1974**, *96*, 1748.

[38] Hoskins, B. F.; Whillans, F. D. *Coord. Chem. Rev.* **1972**, *9*, 365.

largest angle will be 180°, resulting in $\tau = 1$. In most cases of real sp systems, the metal center is displaced out of the basal plane, this will affect the angles in structure, therefore some care is needed in the evaluation of τ and the value τ should not be simply presented as a final answer.

The remainder of the thesis outlines our efforts to synthesize and subsequently characterize Co(II) and Fe(II) complexes bearing the bis(imino)pyridine ligand framework. The general breakdown is presented below.

Chapter 2: A history and synthesis of the bis(imino)pyridine ligand.

Chapter 3: Synthesis of a series of Co(II) bis(imino)pyridine complexes with varied sterics. Ligand-metal interaction and effect of ligand steric bulk on complex stability will be discussed.

Chapter 4: Synthesis of a series Fe(II)bis(imino)pyridine complexes with varied sterics, their characterization, structural analysis and magnetic properties.

Chapter 5: A summary of the work presented in this thesis.

Chapter 2

Bis(imino)pyridine Pincer Ligand Design and Synthesis

[2.1] Introduction

The simplest model of bonding in transition metal complexes is based on the concept that a ligand is a Lewis base (electron pair donor), and the metal is a Lewis acid (electron pair acceptor).[39] In the metal-ligand interaction, the ligand donates one or more electron pairs to the metal center. The result is a Lewis adduct.[40] While this is clearly a simplified approach to metal complex formation, it is a well-established and common starting point in the description and analysis of bonding in coordination complexes.

With the goal of designing single-molecule magnet compounds we targeted five-coordinate complexes of Co(II) and Fe(II). For the structure controlling scaffold to these species we were attracted to the bis(imino)pyridine frame. This family of ligand is defined by its rigid pyridine backbone, and two imine side-arms. Thus, this neutral ligand provides three coplanar nitrogen donors. On each imine group there are two substituents that could be varied; the C-bound groups on the imine backbone (R) or N-bound groups on the side-arms (R`) (Scheme 2.1).

Stoufer and Busch reported the bis(hydrazone)pyridine (Scheme 2.2), the first example of the bis(imino)pyridine class, in 1956. The bis(hydrazone)pyridine was employed

[39] Red Book: IUPAC Nomenclature of Inorganic Chemistry. Third Edition, Blackwell Scientific Publications, Oxford, **1990**, 146.

[40] Crabtree, R, H. In *The Organometallic Chemistry of the Transition Metals*, Fourth Edition, Wiley-Interscience, A John Wiley & Sons.; Inc. Publication, USA, **2005**, 2.

to synthesis of Ni(II), Co(II), and Fe(II) halide complexes.[41] The first bis(arylimino)pyridine (Scheme 2.2) were reported by Alyea and Merrell in 1974. They employed the bis(arylimino)pyridine ligands to synthesize Cu(II), Ni(II), Cd(II), and Zn(II) halide complexes.[42]-[44]

Scheme 2.1

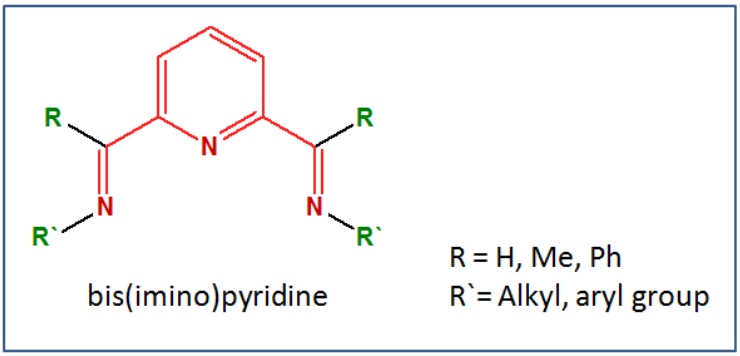

Scheme2.2

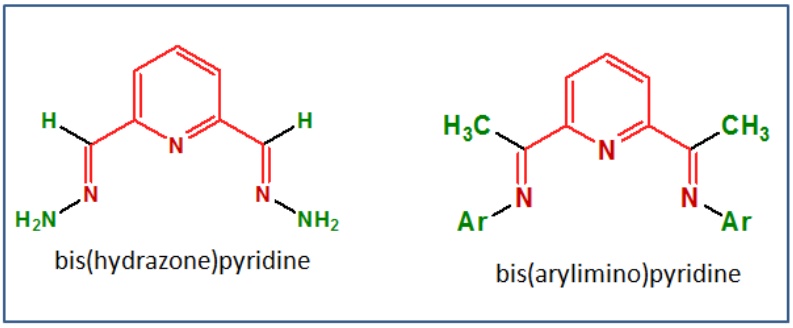

In 1998, Brookhart and Gibson demonstrated the high ethylene polymerization activity of bis(imino)pyridine complexes of Fe(II) and Co(II) dihalides (Scheme 2.3).[45]-[47]

[41] Stoufer, R. C.; Busch, D. H. *J. Am. Chem. Soc*. **1956**, *78*, 6016.

[42] Alyea, E. C.; Merrell, P.H. *Synth. React. Inorg. Met. Org. Chem.* **1974**, *4*, 535.

[43] Alyea, E. C.; Merrell, P. H. *Inorg. Chim. Acta*, **1978**, *28*, 91.

[44] Alyea, E. C.; Ecott, L; Merrell, P. H. *Inorg. Chim. Acta*. **1982**, *59*, 25.

[45] Small, B. L.; Brookhart, M. *J. Am. Chem. Soc*. **1998**, *120*, 7143.

The application of the bis(imino)pyridine ligands was not limited to polymerization activity; and two bis(imino)pyridine ligands have used to synthesize SMMs.[48] Recently, in our group, the bis(imino)pyridine ligand was employed to design and synthesize of Co(II) complexes with the aim of inducing SMM behavior (Scheme 2.4). Bulky ligands induce distortion in the coordination sphere,[49, 50] thereby enhancing spin-orbit coupling, and complexes may exhibit slow magnetic relaxation. Furthermore, the rigid base provided by bis(imino)pyridine ligands could be employed to shift the coordination geometry to a square-pyramidal rather a trigonal bipyramidal.[42]

Scheme 2.3

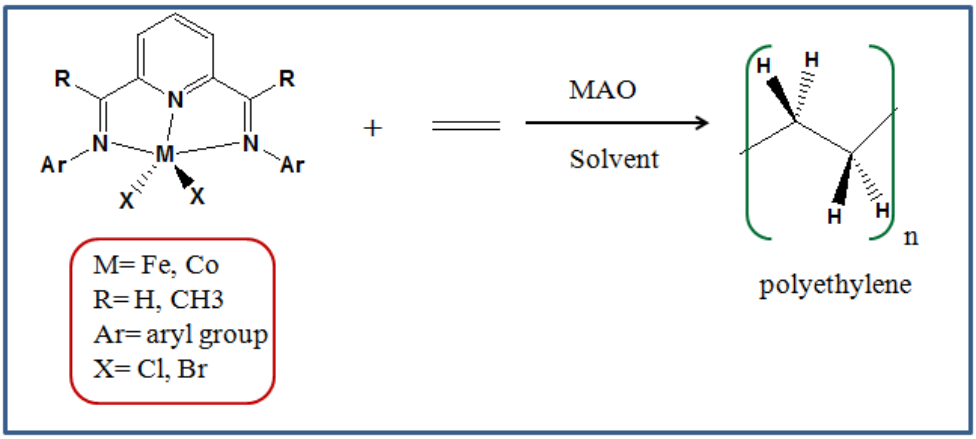

[46] Britovsek, G. J. P.; Gibson, V.C.; Kimberley, B. S.; Maddox, P. J.; McTavish, S. J.; Solan, G. A.;. White, A. J. P; Williams, D. J. *Chem. Commun*. **1998**, 849

[47]Small, B. L.; Brookhart, M.; Bennett, A. M. A. *J. Am. Chem. Soc*. **1998**, *120*, 4049.

[48] Jurca, T.; Farghal, A.; Lin, P. H.; Korobkov, I.; Murugesu, M.; Richeson, D. S.. *J. Am. Chem. Soc.* **2011**, *133*, 15814.

[49] Britovsek, G. J. P.; Bruce, M.; Gibson, V. C.; Kimberley, B. S.; Maddox, P. J.; Mastroianni, S.; McTavish, S. J.; Redshaw, C.; Solan, G. A.; Strömberg, S.; White, A. J. P.; Williams, D. J.; *J. Am. Chem. Soc.* **1999**, *121*, 8728.

[50] Britovsek, G. J. P.; Mastroianni, S.; Solan, G. A.; Baugh, S. P. D.; Redshaw, C.; Gibson, V. C.; White, A. J. P.; Williams, D. J.; Elsegood, M. R. J.; *Chem. Eur. J.* **2000**, *6*, 2221.

The scope of this thesis is to synthesize Fe(II), Co(II) complexes and studying their structural characterization with the goal of understanding how to control single molecule-magnets (SMM) through peripheral ligand modification of the bis(imino)pyridine ligand.

Scheme 2.4

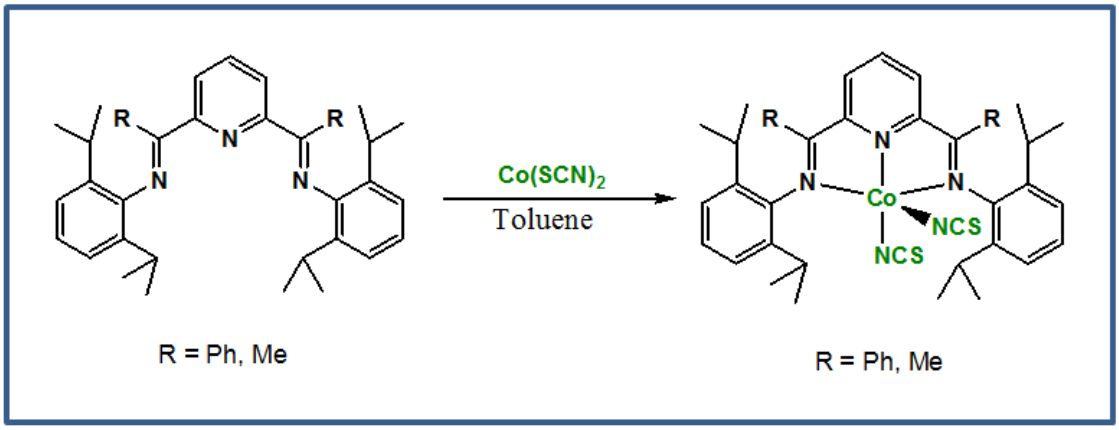

[2.2] Discussion and Synthesis for Bis(imino)pyridine Ligands

In the synthesis of bis(imino)pyridine family, we targeted the synthesis of three less sterically hindered ligands with methyl substituent on the C-imine position (R=CH_3). The ligand **2.1** with the lowest degree of steric bulk was prepared according to the literature;[51] a mixture of (2,6-diacetylpyridine), and excess of aniline was refluxed in propan-2-ol at 100˚C for 2 hours, under a flow of nitrogen (Scheme 2.6). The pale yellow product was washed with hexane to remove aniline impurities, and yielded pure ligand **2.1** (90%).

Scheme 2.6

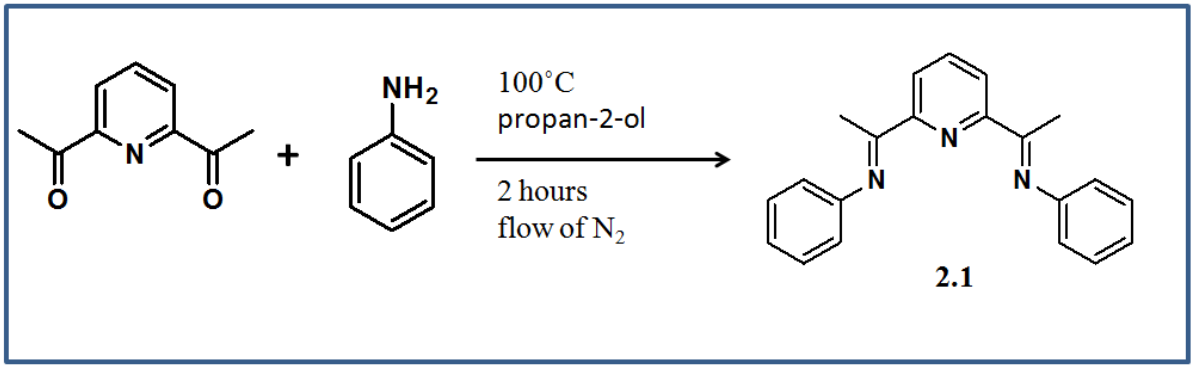

The following reaction procedure was reported by Ying Mu and was used for the synthesis of compounds **2.2** and **2.3**;[52] a mixture of 2,6-diacetylpyridine, aniline, and formic acid was refluxed in methanol at 100˚C for 24 hours, under a flow of nitrogen (Scheme 2.7). The yellow product was washed with hexane to remove aniline impurities, and yielded pure ligand **2.2** (85%) and **2.3** (86%). Synthesis and workup procedure are detailed in section 2.3.

[51] Mentes, A.; Fawcett, J.; Kemmitt, R. D. *Acta Cryst.E.* **2001**, *57*, 424-425

[52] Fan, R.-Q.; Zhu, D.-S.; Mu, Y.; Li, G.-H.; Yang, Y.-L.; Su, O; Feng, S.-H. *Eur. J. Inorg. Chem.* **2004**, 4891.

Scheme 2.7

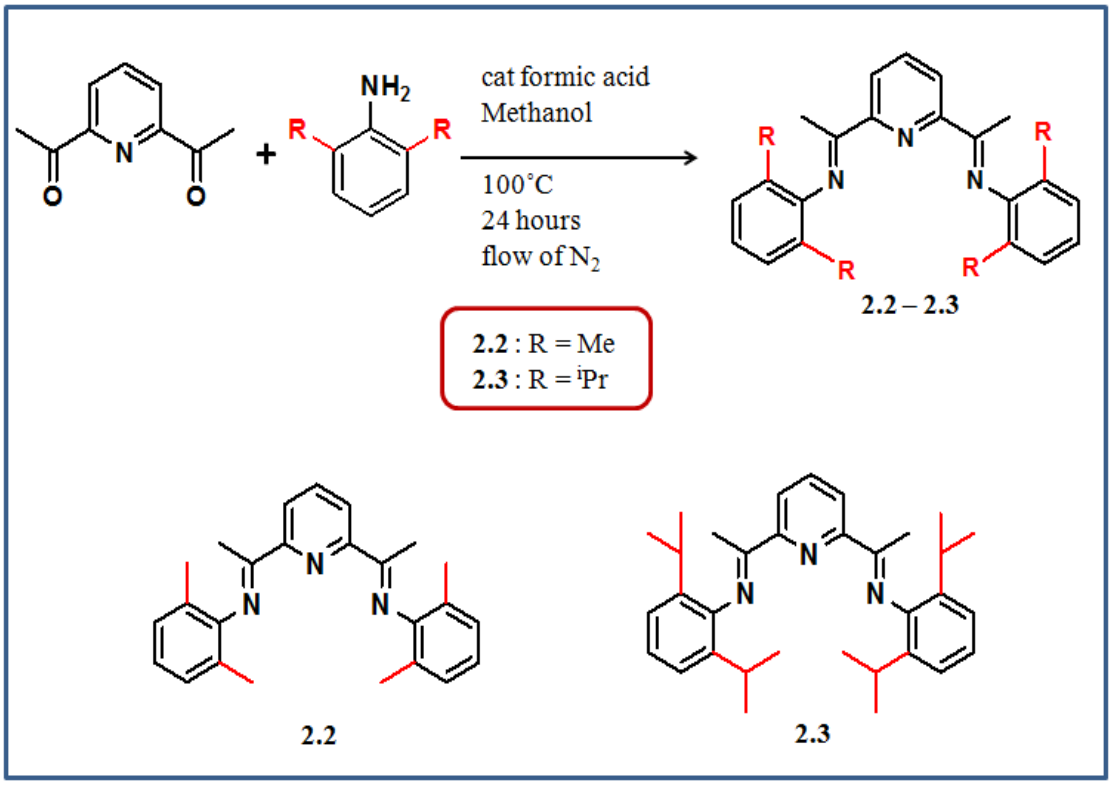

We further functionalized the imine backbone with phenyl groups to increase steric bulk. Following reaction procedure reported by our group for compounds (**2.4**, **2.5** and **2.6**); a mixture of 2,6-dicarbonylpyridine dichloride, aluminum chloride was refluxed in benzene at 100˚C, for 18 hours to generate 2,6-dibenzoylpyridine which is starting material for bis(imino)pyridine synthesis.[53] A mixture of (2,6-dibenzoylpyridine), the appropriate aniline, and p-toluenesulfonic acid was refluxed in toluene at 160˚C for 48 hours, using a Dean-Stark trap, under a flow of nitrogen (Scheme 2.8). The solvent was removed under vacuum to give a yellow oil, the oil dissolved in cold methanol and held at -20˚C for 24 hours to form yellow precipitate. The yellow precipitate was washed with hexane to remove aniline impurities,

[53] Esteruelas, M. A.; Lopez, A. M.; Mendez, L.; Olivan; M.; Onate, E. *Organometallics,* **2003**, *22,* 395.

and yielded pure **2.4** (47%), **2.5** (68%), and **2.6** (67%). Synthesis and purification procedure are detailed in section 2.3.

Scheme 2.8

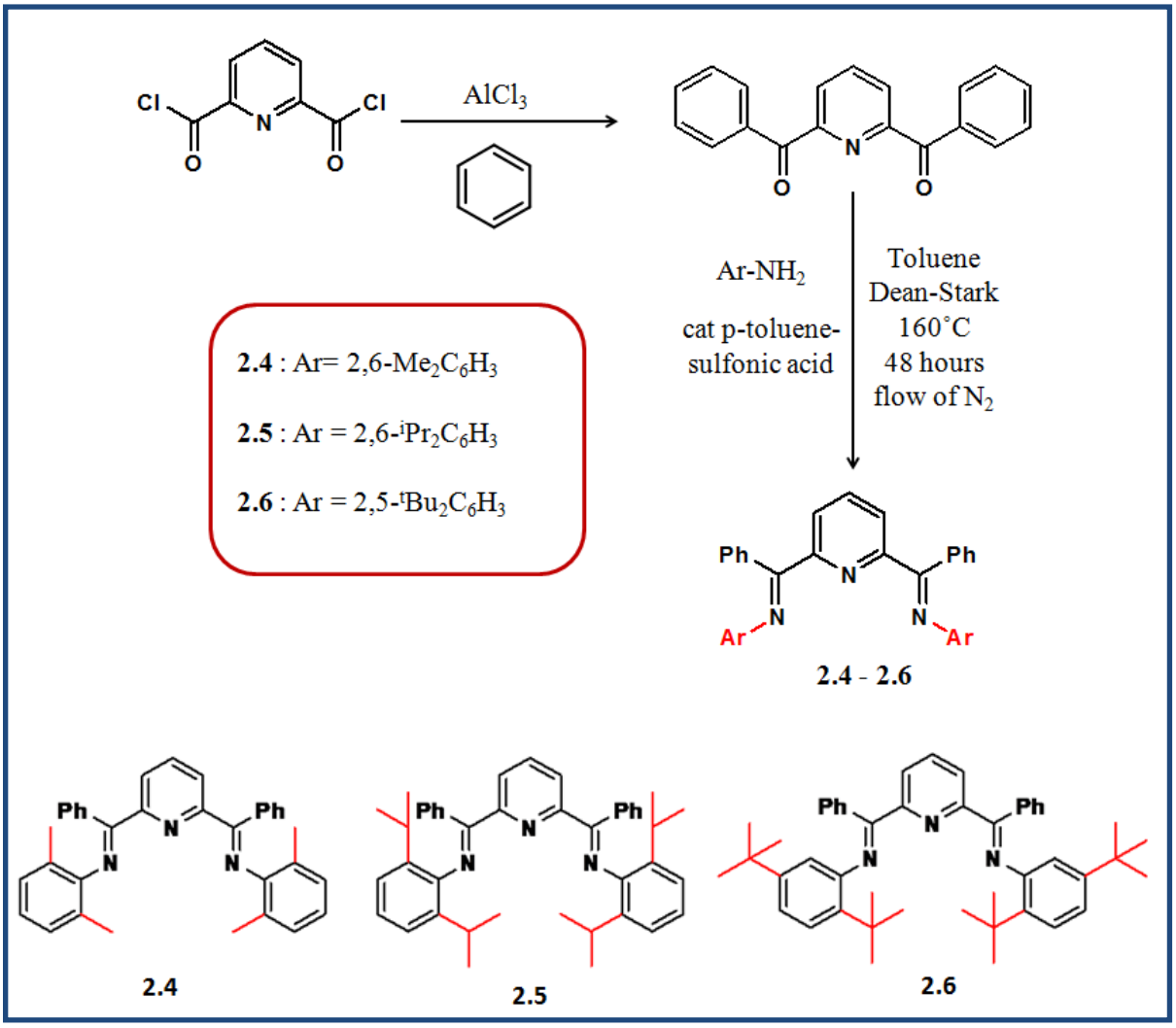

[2.3] Ligand Experimental

General Methods. All reactions were performed using standard Schlenk technique under a flow of nitrogen. All solvents were purchased from Fisher Scientific and all other chemicals were purchased from Aldrich and used without further purification. Compounds **2.1**, **2.2**, **2.3**, **2.4**, **2.5** and **2.6** were synthesis according to published procedure.

(2.1) 2,6-bis[(1-phenylimino)ethyl]pyridine:[54] Aniline (5ml, 55 mmol) was added to a solution of 2,6-diacetylpyridine (0.489 g, 3 mmol) in absolute propan-2-ol (50 mL). The reaction mixture was refluxed for 2 h and then allowed to cool down to room temperature. The crude product precipitated as a yellow powder. Pure **(2.1)** was obtained in 90% yield upon recrystallization from methanol. ^{1}H NMR (60 MHz, $CDCl_3$); δ 8.32 (m, py, 3 H), 7.1 (m, Ph, 10 H), and 2.41 (s, CH3, 6 H) ppm.

(2.2) 2,6-Bis[1-(2,6-dimethylphenylimino)ethyl]pyridine:[52] 2,6-Dimethylaniline (6.4 mL, 51.7 mmol) was added to a solution of 2,6-diacetylpyridine (2.81 g, 17.2 mmol) in absolute methanol (50 mL). After the addition of several drops of formic acid, the reaction mixture was refluxed for 24 h and then allowed to cool down to room temperature. The crude product precipitated as a yellow powder. Pure **2.2** was obtained in 85% yield (5.4 g) upon recrystallization from methanol. ^{1}H NMR (300 MHz, $CDCl_3$): δ 8.56 (d, *J* 7.8 Hz, 2 H, Py-*Hm*), 7.95 (t, *J* 7.8 Hz, 1 H, Py-*Hp*), 7.11-6.95 (m, 6 H, Ar-*H*), 2.27 (s, 6 H, N-C*Me*), 2.07 (s, 12 H, C*Me*) ppm. IR (KBr): ν˜ 3068 (w), 3019 (w), 2970 (w), 2944 (w), 2915 (w), 2851 (w), 2727 (w), 1646 (vs), 1594 (m), 1567 (m), 1468 (s), 1437 (m), 1366 (s), 1324 (w), 1297 (m), 1247 (m), 1203 (s), 1160 (w), 1148 (w), 1126 (s), 1093 (s), 1071 (w), 1029 (w),

[54] Blake, A. J.; Lavery, A. J.; Hyde, T. J.; Schroder, M. *J. Chem. Soc. Dalton Trans*. **1989**, 965.

991 (w), 972 (w), 920 (w), 886 (w), 875 (w), 826 (s), 817 (s), 804 (w), 777 (s), 762 (vs), 744 (w), 692 (m), 623 (m), 576 (w), 541 (w), 530 (w), 493 (w), 422 (w) cm^{-1}. $C_{25}H_{27}N_3$ (369.5): calcd. C 81.26, H 7.37, N 11.37; found C 80.98, H 7.40, N 11.56.

(2.3) 2,6-Bis[1-(2,6-diisopropylphenylimino)ethyl]pyridine:[52] 2,6-Diisopropyl aniline (8.7 mL, 46.1 mmol) was added to a solution of 2,6-diacetylpyridine (2.5 g, 15.3 mmol) in absolute methanol (50 mL). After the addition of several drops of formic acid, the reaction mixture was refluxed for 24 h and then allowed to cool down to room temperature. The crude product precipitated as yellow powder. Pure **2.3** was obtained in 86% yield (6.35 g) upon recrystallization from methanol. ^{1}H NMR (300 MHz, $CDCl_3$): δ 8.60 (d, *J* 7.8 Hz, 2 H, Py-*Hm*), 7.98 (t, *J* 7.8 Hz, 1 H, Py-*Hp*), 7.21-7.13 (m, 6 H, Ar-*H*), 2.78 (sept, *J* 6.8 Hz, 4 H, C*H*Me_2), 2.30 (s, 6 H, N-C*Me*), 1.19 (dd, *J* 6.8 Hz, 24 H, CH*Me*$_2$) ppm. IR (KBr): $\tilde{\nu}$ 3068 (w), 2960 (s), 2925 (w), 2870 (w), 1646 (vs), 1588 (w), 1571 (w), 1455 (m), 1438 (m), 1406 (w), 1383 (w), 1368 (s), 1321 (w), 1301 (w), 1255 (w), 1240 (m), 1195 (m), 1121 (m), 1103 (w), 1079 (w), 1059 (w), 1041 (w), 994 (w), 961 (w), 936 (w), 886 (w), 829 (m), 801 (w), 770 (s), 758 (w), 744 (w), 691 (w), 634 (w), 533 (w), 443 (w) cm^{-1}. $C_{33}H_{43}N_3$ (481.7): calcd. C 82.28, H 9.00, N 8.72; found C 82.50, H 8.91, N 8.65.

(2.4) 2,6-Bis{1-[(2,6-dimethylphenyl)imino]-benzyl}pyridine:[55] A mixture of 2,6-dibenzoylpyridine (1.0 g, 3.48 mmol), an excess of 2,6-dimethylaniline (1.10 g, 9.08 mmol), p-toluenesulfonic acid (0.1 g) in toluene (150 mL) were placed in a round-bottom flask under nitrogen atmosphere, and the reaction flask was equipped with a Dean-Stark trap. The reaction mixture was heated to160˚C, using a sand bath, for 48 h. The workup was

[55] Jurca, T.; Korobkov, I.;.Yap, G. P. A.; Gorelsky, S. I.; Richeson, D. S. *Inorg. Chem*. **2010**, *49*, 10635.

performed under lab atmosphere conditions. The reaction mixture was cooled to room temperature, and the solvent was removed under vacuum to give a dark yellow oil. Cold methanol was added to this oil, and the solution was held at -20˚C for 24 h, over which time a bright yellow precipitate formed. The precipitate was removed by filtration, and washed with cold methanol and hexanes to afford a fine yellow powder. The powder was further purified by flashing through a silica plug with 15:1 hexanes/ethyl acetate. The solvent was removed under the vacuum to afford a very fine yellow powder in moderate 47% yield (809 mg, 1.64 mmol), but in high purity. Analysis for $C_{35}H_{31}N_3$ Calculated: C, 85.16; H, 6.33; N, 8.51 Found: C, 85.30; H, 6.47; N, 8.41. Room temperature ^{1}H NMR ($CDCl_3$, 300 MHz) and ^{13}C NMR ($CDCl_3$, 75 MHz) showed a number of resonances which could not be properly assigned and were attributed to a fluxional species. ^{1}H NMR (T=115˚C, d_6-dimethyl sulfoxide, 300 MHz) δ 8.20- 7.65(brm, 3 H, py, CH), 7.39 (v br s, 10H, Ar-H), 6.89 (br m, 6H, Ar-H), 1.99(m, 12H,CH_3). ^{13}C NMR (T=115˚C, d_6-dimethyl sulfoxide, 75 MHz) δ 165.7 (C=N imine), 155.2(py-C), 148.6(Ar-CH), 137.5(Ar-C), 136.9(Ar-CH), 130.3(Ar-C), 128.5(Ar-CH), 128.2(Ar-CH), 127.6(Ar-CH), 125.3(Ar-CH), 122.9(Ar-CH), 122.7(A-C), 18.1(-CH_3).

(2.5) 2,6-Bis{[2,6-di(isopropyl)phenyl)imino]benzyl}pyridine:[56] A mixture of 2,6-dibenzoylpyridine (5.0 g, 17.4 mmol), 2,6-diisopropylaniline (7.5 g, 38.3 mmol), and p-toluenesulfonic acid (0.2 mg) in toluene (50 mL) were placed in a round bottom flask equipped with a Dean–Stark trap. Under a nitrogen atmosphere, the reaction mixture was heated to reflux in an oil bath at 140˚C for 48 h then cooled to room temperature and the solvent was removed under vacuum to give a dark yellow oil. Hexanes were added and a

[56] Jurca, T.; Dawson, K; Mallov, I.; Burchell, T; Yap, G. P. A.; Richeson, D. S. *Dalton Trans*, **2010**, *39*, 1266.

small quantity of a white solid was removed by filtration. The filtrate was removed under vacuum yielding a dark yellow oil. Methanol (~400 mL) was added to this oil and the mixture was stirred for several minutes, causing the product to precipitate as a yellow solid which was filtered off and rinsed with methanol. The filtrate was reduced to about half the initial volume under vacuum, and then placed in a refrigerator, causing additional product to precipitate, which was filtered off and rinsed with methanol. The product was obtained as a yellow powder. Yield: 7.2 g (68%). Elemental analysis for $C_{43}H_{47}N_3$ Calculated: C, 85.25; H, 7.82; N, 6.94 Found: C, 85.08; H, 7.69; N, 6.86. MS (EI) *m*/*z* 605 (M+). ^{1}H NMR(*T* = 115˚C, d_6-dimethyl sulfoxide, 300 MHz) *d* 7.82 (br t, 1 H, py, *p*-CH), 7.55–7.20 (br m, 12 H, Ar–H), 6.94 (br s, 6H, Ar–H), 2.90 (m, 4H, ^{i}Pr), 1.00 (d, 24H, ^{i}Pr). ^{13}C NMR (*T* = 115˚C, d_6-dimethyl sulfoxide, 75 MHz) *d* 164.6 (C=N imine), 155.2 (py, *o*-C=N), 146.2 (Ar-CH), 136.8 (Ar-*i*-C), 135.5 (Ar-CH), 130.1 (Ar-CH), 128.9 (Ar-CH), 128.1 (Ar-CH), 123.7 (Ar-CH), 123.2 (Ar-CH), 122.7 (Ar-CH), 28.2 (Ar-^{i}Pr, CH-$(CH_3)_2$), 22.9 (Ar-^{i}Pr, CH3), 22.3 (Ar-^{i}Pr, CH_3).

(2.6) 2,6-Bis{1-[(2,5-ditertbutylphenyl)imino]-benzyl}pyridine:[56] The synthetic procedure was adapted from literature preparation described by Kleigrewe *et al.*[57] Under lab atmosphere, a 250 mL round bottom flask was charged with 2,6-dibenzoylpyridine (5.4 g 18.8 mmol), 2,5-di-*tert*-butylaniline (7.4 g, 41.4 mmol), and *p*-toluenesulfonic acid (0.1 g) in toluene (150 mL). A Dean–Stark trap was attached to the flask and the reaction mixture was placed under nitrogen atmosphere and heated to reflux (140˚C) for 48 h. Over this time, the reaction mixture became brown and a brown precipitate formed. The mixture was concentrated *in vacuo*, resulting in a thick brown paste, which was subsequently dissolved in

[57] Kleigrewe, N.; Steffen, W.; Blomker, T.; Kehr, G.; Frohlich, G; Wibbeling, B.; Erker, G.; Wasilke, J.C; Wu, G.; Bazan, G. G. C. *J. Am. Chem. Soc.*, **2005**, *127*, 13955.

cold methanol to give a yellow precipitate. The yellow solid was collected by filtration and washed with a minimal amount of cold hexanes : ether (9 : 1) to remove aniline impurities. The filtrate was reduced again to a thick paste and this procedure was repeated several times. Compound **2.6** was isolated as a bright yellow powder in 67% yield (8.377 g). Analysis calcd for $C_{47}H_{55}N_3$: C, 85.28; H, 8.37; N, 6.35. Found: C, 84.68; H, 8.73; N, 6.12. MS (EI) *m*/*z* 605 (M+). Room temperature NMR spectra, 1H NMR ($CDCl_3$, 300 MHz) and 13CNMR($CDCl_3$, 75 MHz), displayed a complex array of resonances which could not be completely assigned due to rotational conformers. NMR spectra obtained at 115˚C resulted in simplification of the spectra. ^{1}H NMR (d_6-dimethyl sulfoxide, 500 MHz, T = 115˚C) d 8.20–6.90 (br m, 17 H, Ar–H), 6.21 (br s, 2H, Ar–H), 1.39 (br s, 18H, ^{t}Bu), 0.99 (br s, 18H, ^{t}Bu). ^{13}C NMR (d_6-dimethyl sulfoxide, 125 MHz, T = 115˚C) d 148.5 (Ar-CH), 147.9 (Ar-CH), 138.7 (Ar-CH), 129.1 (Ar-CH), 128.4 (Ar-CH), 128.3 (Ar-CH), 126.1 (Ar-CH), 120.8 (Ar-CH), 118.8 (Ar-CH), 131.6 (Ar-CH), 99.9 (Ar-CH), 35.0 (Ar-^{t}Bu, C-$(CH_3)_3$), 33.8 (Ar-^{t}Bu, C-$(CH_3)_3$), 31.1 (Ar-^{t}Bu, CH3), 30.5 (Ar-^{t}Bu, CH_3).

Chapter 3

Synthesis and Characterization of Co(II) Complexes with the Bis(imino)pyridine Ligand Framework.

[3.1] Introduction

Molecules with a high degree of magnetic anisotropy can behave as single-molecule magnets (SMMs). This refers to the fact that such species have a predisposition to maintain a direction to the overall electronic spin of the molecule. Since the first SMM behaviors were observed in transition metal cluster [58] - [62], such as polynuclear complex $[Mn_{12}O_{12}(CH_3COO)_{16}(H_2O)_4]$, many research groups have been searching for new polynuclear systems in the hope of devising high-temperature applications. Current SMMs function below 10 K. The general goal has been to increase the total spin of the molecules (*S*) by adding more paramagnetic centres to the complexes. The best results to-date are for a hexametallic manganese compound, $[Mn_6O_2(Et\text{-}sao)_6(PhCOO)_2]$ (Et-sao: ethyl-salicyladoxime) has energy barrier to magnetisation of 86 K..

---

[58] Milios, C. J.; Vinslava, A.; Wernsdorfer, W.; Moggach, S.; Parsons, S.; Perlepes, S. P.; Christou, G.; Brechin, E. K. *J. Am. Chem. Soc*. **2007**, *129*, 2754.

[59] Christou, G.; Gatteschi, D.; Hendrickson, D. N.; Sessoli, R. MRS Bull. **2000**, *25*, 66.

[60] Thomas, L.; Lionti, L.; Ballou., R.; Gatteschi, D.; Sessoli, R.; Barbara, B. *Nature* **1996**, *383*, 145.

[61] Maheswaran, S.; Chastanet, G.; Teat, S. J.; Mallah, T.; Sessoli, R.;Wernsdorfer, W.; Winpenny, R. E. P. *Angew. Chem*. **2005**, *44*, 5044.

[62] Sokol,J. J.; Hee, A. G.; Long, J. R. *J. Am. Chem. Soc*. **2002**, *124*, 7656.

In addition to the total spin (*S*), the height of the anisotropy barrier (to spin reversal) also depends on the zero-field splitting (ZFS) parameter *D***.** Spin-orbit effects can be the primary contributor to make ZFS quite large. It is also important to realize that, in addition to the thermal crossing of the barrier, the spin direction can be changed (relaxed) by tunneling effects that are usually related to the rhombic ZFS parameter represented by **E**.

In 2003 a monomeric anion complex, $[TbPc_2]^-$, which possesses only one Tb(III) cation, was reported to exhibit slow magnetization relaxation together with a huge anisotropic barrier. Several mononuclear lanthanide complexes of Er(III) and Dy(III) as well as some actinide species, with U(III) and Np(III) have shown similar SMM behaviour. These results point to the role of metals with large spin-orbit effects in displaying SMM behavior.

Recently the SMM behavior have been demonstrated by Chang, Long and co-workers for mononuclear Fe(II) (high spin, $S = 2$) complex. In these mononuclear SMMs, the highly anisotropic ground state is attributed to the strong spin-orbit coupling.[63] In these compounds, spin-orbit coupling was enhanced by structural distortions within the coordination geometry. Motivated by this idea, we sought to expand bis(imino)pyridine chemistry towards the synthesis of mononuclear Co(II) complexes.

Co(II) has an inherently high magnetic anisotropy among the first row transition metals. Two coordination geometries are associated with five coordinate Co(II), the first is trigonal bipyramidal (tbp), and the second is square pyramidal (sp). The orbital configuration for ideal tbp and sp is shown in Figure 3.1. In ideal trigonal bipyramidal and square

[63] Mabbs, F. E.; Machin, D. J.; In *Magnetism and Transition Metal Complexes*. **2008**. Dover Publications.

pyramidal coordination geometry, orbital configuration for high-spin cobalt(II) center (S = 3/2), reveals no spin-orbit coupling (no orbital contribution possible due to degenerate orbitals are completely occupied).

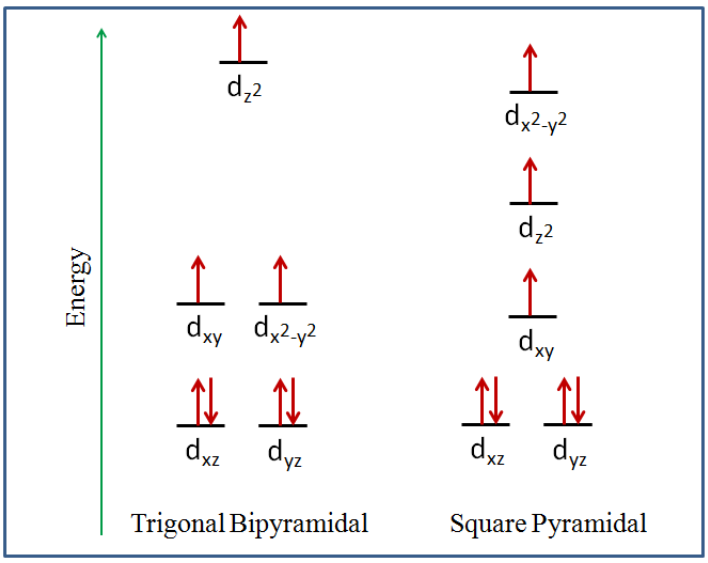

Figure 3.1: Splitting of the 3d orbital energies for a high-spin Co(II) center in a trigonal bipyramidal (left) and square pyramidal (right) ligand field.

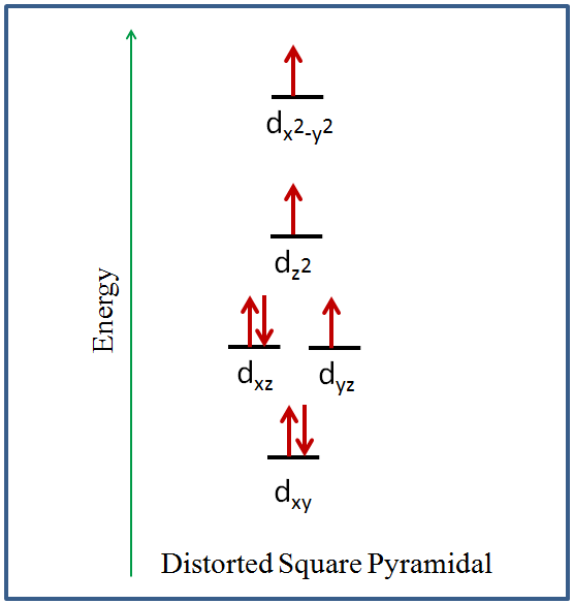

Figure 3.2: Splitting of the 3d orbital energies for a high-spin Co(II) center in a distorted square pyramidal ligand field.

The use of a bis(imino)pyridine ligand in the synthesis of Co(II) complexes form high-spin molecules.[64]-[69] In addition, this bulky ligand scaffold induces distortion in the coordination geometry.[70,71] The structural distortions within the five coordination geometry induce spin-orbit coupling. For example, the orbital configuration for high-spin Co(II) in distorted sp geometry reveals spin-orbit coupling between degenerate orbitals (Figure 3.2). Spin-orbit coupling enhances magnetic anisotropy, resulting in slow magnetic relaxation.

Our goal is to synthesize and characterize the bis(imino)pyridine complexes of Co(II), and to better understand how to enhance magnetic anisotropy by controlling the metal coordination geometry through modification of bis(imino)pyridine ligand.

For the remaining two coordination sites several different ligands were chosen: bromide, isothiocyanide, and cyanide ligands. These anions are located on the left, middle, and right of spectrochemical series respectively (Figure 3.3). These monodentate ligands allow for flexibility in metal environment and their differences in ligand field strength will allow us to probe the role of these species on the splitting pattern in Figure 3.2.

---

[64] Bianchini, C.; Gatteschi, D.; Giambastiani, G.; Guerrero Rios, I.; Ienco, A.; Laschi, F.; Mealli, C.; Meli, A.; Sorace, L.; Toti, A.; Vizza, F. *Organometallics.* **2007**, *26*, 726.

[65] Bianchini, C.; Mantovani, G.; Meli, A.; Migliacci, F. *Organometallics*. **2003**, *22*, 2545.

[66] Sun, W.-H.; Tang, X.; Gao, T.; Wu, B.; Zhang, W.; Ma, H. *Organometallics*. 2004, 23, 5037.

[67] Champouret, Y. D. M.; Fawcett, J.; Nodes, W. J.; Sing, K.; Solan, G. A.; *Inorg. Chem*. **2006**, *45*, 9890.

[68] Bianchini, C.; Giambastiani, G.; Guerrero Rios, I.; Meli, A.; Oberhauser, W.; Sorace, L.; Toti, A. *Organometallics*. **2007**, *26*, 5066.

[69] Barbaro, P.; Bianchini, C.; Giambastiani, G.; Guerrero Rios, I.; Meli, A.; Oberhauser, W.; Segarra, A. M.; Sorace, L.; Toti, A.; *Organometallics*. **2007**, *26*, 4639.

[70] Small, B. L.; Brookhart, M.; Bennett, A. M. A. *J. Am. Chem. Soc*. **1998**, *120*, 4049.

[71] Bennett, A. M. A.; DuPont; WO Patent. **1998**, *98*, 27124.

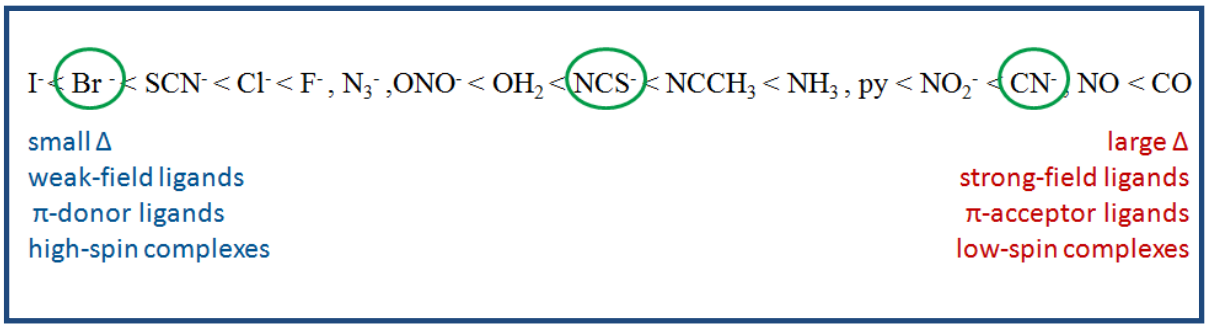

Figure 3.3: A partial spectrochemical series of ligands from small Δ to large Δ.

[3.2] Results and Discussion: Synthesis and Characterization

Reaction of $Co(SCN)_2$ with ligands **2.2**, **2.4** and **2.6**, shown in Scheme 3.1, directly produces the targeted Co(II) complexes of these ligands as green powder **3.1** (70%), **3**.2 (96%), and **3.3** (69%). Microanalyses support the formation of these formulations as 2,6-$\{[(R_2C_6H_3)N]CR'\}_2C_6H_3N]Co(II)(NCS)_2$ (R = Me, ^{i}Pr, ^{t}Bu; R' = Me or Ph). The molecular structures of these compounds were confirmed through single crystal X-ray analysis as summarized in Tables 3.1, 3.2 and 3.3, and Figures 3.4, 3.5, 3.9. Compounds **3.4** and **3.5** were synthesized in high yield according to published procedures (Scheme 3.2).[49,72]

Compounds **3.1**, **3.2**, **3.3**, **3.4**, and **3.5** display analogous bis(imino)pyridine Co(II) bis(thiocyanate) structures that have five-coordinate metal centers (Scheme 3.1 and 3.2). The bis(imino)pyridine ligand backbone is π-conjugated and the most stable structure should be planar. In all cases the bis(imino)pyridine ligand is coordinated as a tridentate pincer ligand and the thiocyanates are coordinated through the N centers (isothiocyanate). The ligand coordinates to the Co(II) center to generate two five-membered rings with bite angles N(im)

[72] Sacconi, L.; Morassi, R.; Midollini, S. *J. Chem. Soc. A*. **1968**, 1510.

-N(py) that range in these compounds from 74°-76.3°. This is an inherent limit that leads to some deviations from ideal metal coordination geometry.

Scheme 3.1

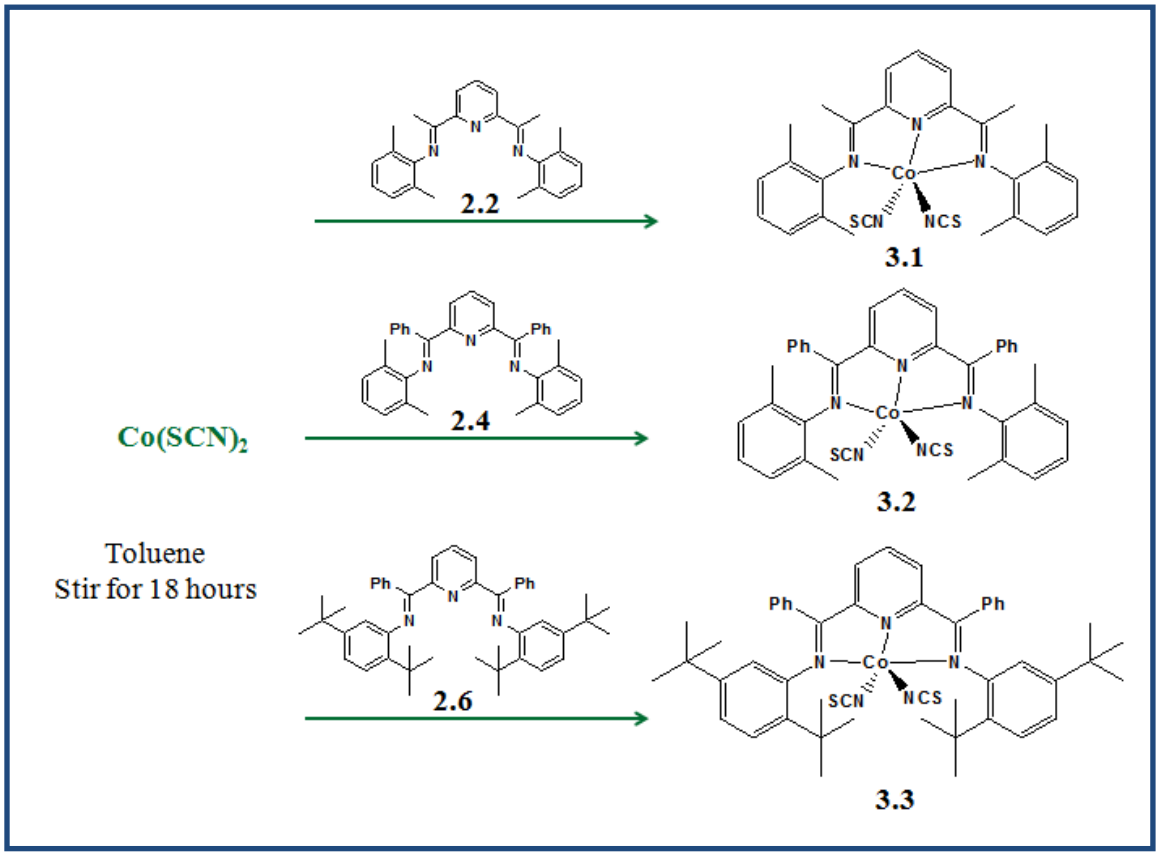

Scheme 3.2

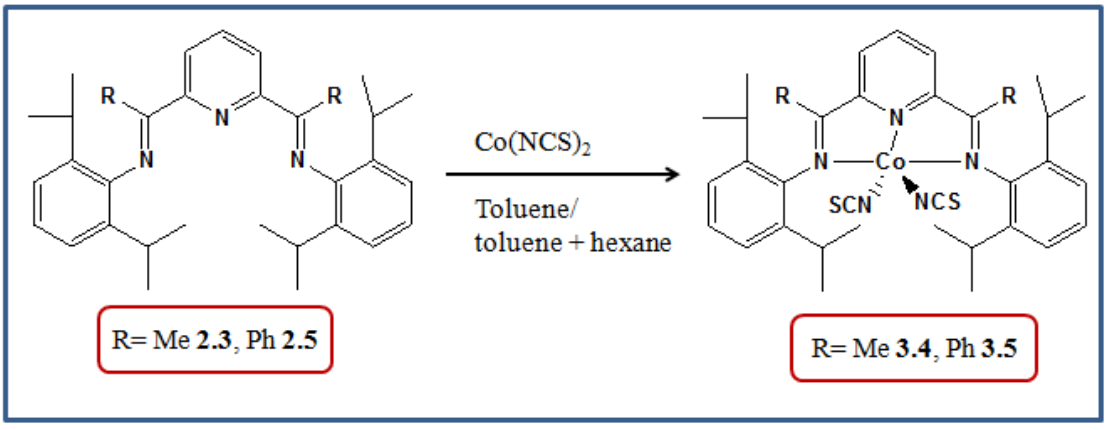

The cobalt-ligand bond lengths are comparable between these compounds as summarized in Table3.4 The only real differences is the two Co-NCS bonds. In **3.3**, **3.4**, and **3.5** where a clear axial site can be identified, the axial ligand is longer but in **3.1** and **3.2**, which appear to be more trigonal bipyramidal with both NCS anions in the equatorial sites, the two Co-NCS bonds are identical within error.

Table 3.4. The cobalt-ligand bond lengths (Å) for **3.1**, **3.2**, **3.3**, **3.4**, and **3.5.**

	3.1		**3.2**		**3.3**		**3.4**		**3.5**	
Co-NCS	Co(1) -N(5)	1.950 (3)	Co(1) -N(4)	1.957 (4)	Co(1) -N(4)	1.931 (6)	Co(1) -N(4)	1.948 (4)	Co(1)- N(3)	1.949 (5)
Co-NCS	Co(1) -N(4)	1.957 (3)	Co(1) -N(5)	1.967 (4)	Co(1) -N(5)	2.002(9) Axial	Co(1) -N(5)	1.993(4) axial	Co(1)- N(4)	1.968 (5) axial
Co-Npy	Co(1) -N(2)	2.020 (2)	Co(1) -N(2)	2.025 (3)	Co(1) -N(2)	2.044 (4)	Co(1) -N(2)	2.054 (3)	Co(1)- N(2)	2.044 (3)
Co-Nim	Co(1) -N(1)	2.188 (2)	Co(1) -N(3)	2.231 (4)	Co(1) -N(3)	2.152 (5)	Co(1) -N(1)	2.153 (3)	Co(1)- N(1)	2.222 (3)
Ci-Nim	Co(1) -N(3)	2.236 (2)	Co(1) -N(1)	2.246 (4)	Co(1) -N(1)	2.219 (4)	Co(1) -N(3)	2.159 (3)	-	-

The structures of the $Co(SCN)_2$ complexes of bis(imino)pyridine ligands can be described using defined molecular planes. A common plane to all of them can be defined by the cobalt center and the three coordinated nitrogen centers of the pyridyl group [N(py)] and the two isothiocyanate groups [N(thio1) and N(thio2)]. This plane contains the metal center and bisects the bis(imino)pyridine ligand. Another plane that is useful in the geometry description is one that is defined by the three N centers of the bis(imino)pyridine ligand and the isothiocyanate that is approximately trans to the pyridyl moiety [e.g. N(im)-N(py)-

N(im)-N(thio1)]. This is the plane that would define the basal plane in a distorted square pyramidal coordination geometry.

Compounds **3.1** and **3.3** appear to most clearly represent the limits of the five-coordinate geometry; the first is a distorted trigonal bipyramidal complex and the second is a distorted square pyramidal species.

Compound **3.1** has the formula 2,6-{[$(Me_2C_6H_3)$N]CMe}$_2C_5H_3$NCo(II)$(NCS)_2$ and represents the compound in this group with the least sterically encumbering substituents (Figure 3.4). The plane defined by the nitrogen atoms of the pyridyl group and the two thiocyanates [N(2), N(4), N(5)] beautifully bisects the molecule and is at an angle of 87.2° with the mean plane of the ligand defined by the pyridyl N and the two imine N atoms [N(1), N(2), N(3)]. Defining a mean plane that uses the three bis(imino)pyridine nitrogens and one of the thiocyanate N centers, is less appealing. This approach generates a plane that does not align with the ligand backbone plane and does not appear to reflect much of the molecular symmetry.

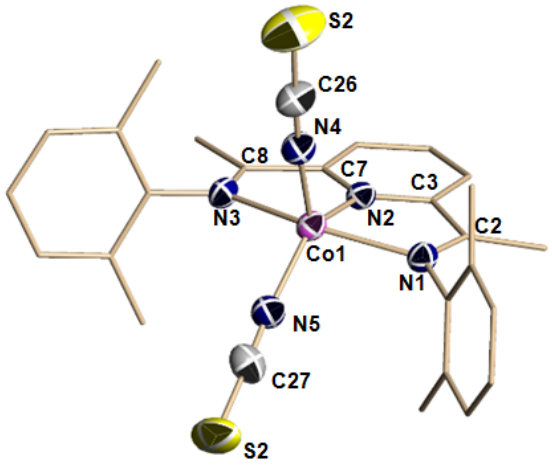

Figure 3.4 : X-ray structure of compound **3.1** with hydrogen atoms and CH_2Cl_2 omitted for clarity. Select bond lengths and angles are given in Tables 3.2 and 3.3.

While the tau (τ) angle is the common method to analyze a five-coordinate structure, the value of this parameter is somewhat limited in this case due to the bite angle limitations of the pincer bis(imino)pyridine ligand. For example in this compound the calculated τ parameter of N(1)-Co(1)-N(3) as the axial/largest angle 150.26°(9) and the next larger of the remaining three angles [N(5)-Co(1)-N(2) = 137.58°(11)], obtain a τ = 0.211. While closer to 0 than 1, this is not very satisfying. The angles of the N(py)-Co-N(thio) indicate a structure of a distorted trigonal bipyramid. In a full square pyramidal species these values should be 180° and 90° and in a tbp they should be equal and 120°. In this compound the two angles are [N(2)-Co(1)-N(4) = 113.31°(10)] and [N(2)-Co(1)-N(5) = 137.58°(11)]. These two angles differ from 120° (tbp) by 6.7, 17.6 degrees while they differ from 180° and 90° by 42.4°, 23.3°. This clearly suggests the deviation it toward the tbp geometry.

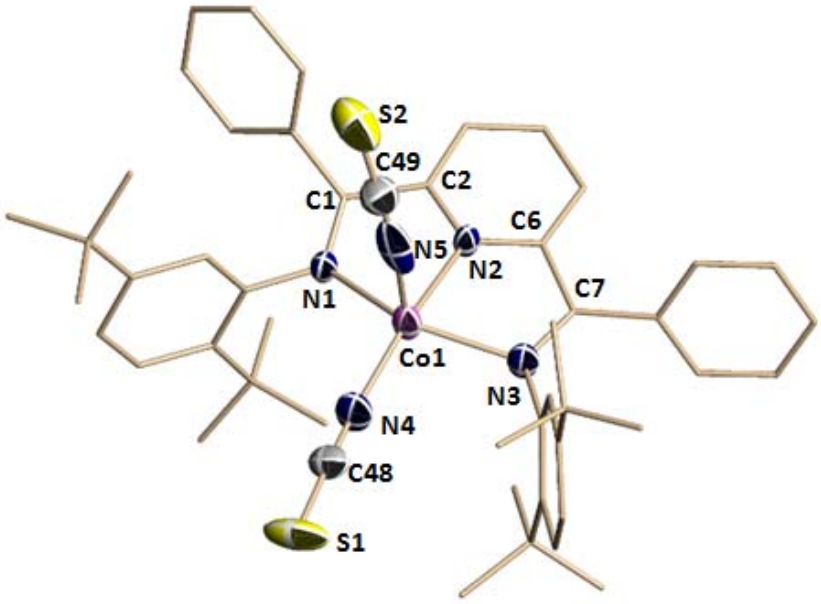

Figure 3.5 : X-ray structure of compound **3.3** with hydrogen atoms omitted for clarity. Select bond lengths and angles are given in Tables 3.2 and 3.3.

Compound **3.3** has the formula 2,6-{[(^{t}Bu$_2$C$_6$H$_3$)N]CPh}$_2$C$_5$H$_3$NCo(II)(NCS)$_2$ and represents the compound in this group with the most sterically encumbering substituents **(**Figure 3.5). This structure looks the most like a square pyramid with a plane defined by the three bis(imino)pyridine nitrogen centers and one thiocyanate group [i.e. N(1), N(2), N(3), N(4)] (Figure 3.6). There is a nearly perpendicular plane (84.7°) defined by N(2), N(4), N(5). In this case the ligand backbone is close to being coplanar with the N(1), N(2), N(3), N(4) plane with a small twist along the M-N(py) axis. The Co center deviates slightly above the basal plane defined by N(1), N(2), N(3) and N(4) at a distance of only 0.36 Å. In addition the nearly linear thiocyanate N(4)-C(48)-S(1) is in this plane with the S(1) atom just 0.20 Å above the plane. The N-Ar groups are perpendicularly oriented to the ligand plane and are approximately bisected by it. There does appear to be a slight twist that pushes the t-Bu groups on one side of the molecule into the open/empty site on Co. The thiocyanates are nearly linear with the angles at [N(4) = 167.4°] , the angle at [C(48) = 177.7°], the angle at [N(5)=166.2°] and the angle at [C(49)= 178.9°].

The τ parameter calculation for this compound would be based on an α (largest) angle of [N(4)-Co(1)-N(2) = 167.7°(2)] while the beta angle would be defined as [N(3)-Co(1)-N(1) = 139.90°(18)], this gives a value of τ = 0.4633. This is not very valuable since it is in between the value of 0 and 1. By inspection this compound looks square pyramidal. As with compound **3.1** the angles of the N(py)-Co-N(thio) groups help with this analysis. In a full square pyramid these values should be 180° and 90° , and in a tbp they should be equal and 120°. In this compound the [N(2)-Co(1)-N(4) = 167.7°(2)] and [N(2)-Co(1)-N(5) = 88.0°(2)]. These two angles differ from the square pyramidal value by only by 12.3, 2.0 degrees. As a result this compound **3.3** is best described as distorted square pyramidal

geometry in which the coordinated nitrogen atoms from the chelate ligand and from one isothiocyanate form the base. The second isothiocyanate ligand lies in the apical position[73].

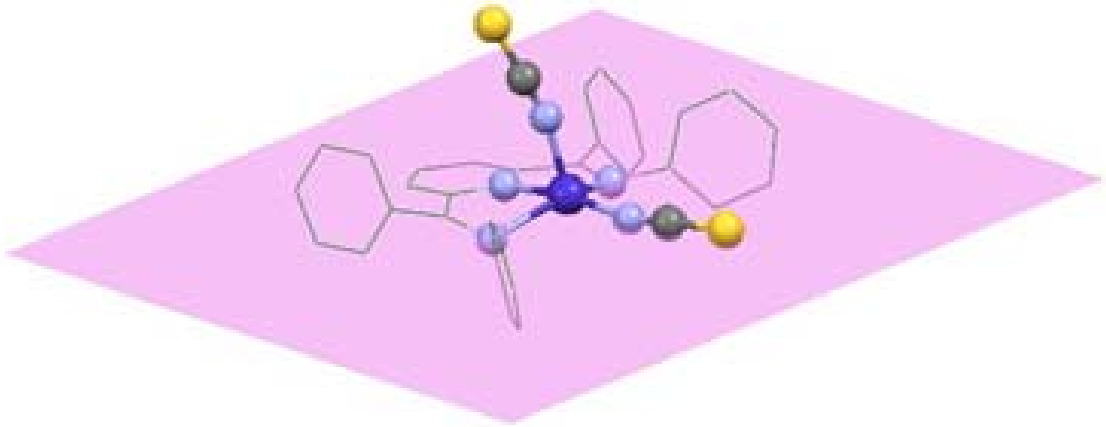

Figure 3.6 : X-ray structure of **3.3** with hydrogen atoms and ^{t}Bu groups omitted for clarity. Plane defined by the three bis(imino)pyridine nitrogen centers and one thiocyanate group.

Compound **3.4** has the formula 2,6-{[(iPr$_2$C$_6$H$_3$)N]CMe}$_2$C$_5$H$_3$NCo(II)(NCS)$_2$ and coordination geometry looks more like compound **3.3** with the cobalt in a distorted square pyramidal environment **(**Figure 3.7**)**. Cobalt sits above the basal mean plane defined by N(1), N(2), N(3), N(4) by 0.39 Å. This plane also contains the ligand framework and the pyridine ring carbons. The isopropyl phenyl groups twist out of the plane slightly such that the para C are symmetrically directed below the plane. This tipping moves an ^{i}Pr group on each into the open faces of the Co. The thiocyanate ligand also points down slightly below the plane with S (- 0.43 Å) relative to the plane. The thiocyanates are close to linear with the angles around N (168.7°, 173.9°) and C (179.6°, 179.1°) being nearly 180°. A perpendicular molecular

[73] Kooistra, T. M.; Hekking, K. F. W.; Knijnenburg, Q.; de Bruin,B.; Budzelaar, P. H. M.; de Gelder, R.; Smits, J. M. M.; Gal, A. W. *Eur. J. Inorg. Chem*. **2003**, 648.

plane can be defined by N(2), N(4), N(5), it is at 89.2° from first plane. These are the angles to define square pyramid like with compound **3.3**.

Compound **3.5** has the formula 2,6-{[(^{i}Pr$_2$C$_6$H$_3$)N]CPh}$_2$C$_5$H$_3$NCo(II)(NCS)$_2$ like compound **3.4** but the carbon substituent is now R = Ph (Figure 3.8). This increased steric load leads to a more pronounced distortion with the metal center lying out of the basal plane defined by N(1), N(2), N(1'), N(3) by 0.52 Å. The pyridyl group (e.g. the C atoms) lies in the plane. The 2,6-diisopropyl)phenyl substituents on the coordinated imine nitrogen centers lie orthogonal to the basal plane of the complex and their orientation is very similar to compound **3.4** (i.e rotated in the same fashion). Also, like compound **3.4,** the phenyl substituents of the iminocarbon atoms are clearly rotated out of the plane of the Schiff base functional groups, to avoid steric interaction with the bulky aryl substituents and contact with the central pyridyl group. Also like compound **3.4**, the isothiocyanate ligand that is in the basal plane tips down below the plane. In this case further below the plane (S(1) to plane is 1.50 Å below) consistent with a larger steric load for the bis(imino)pyridine ligand. The thiocyanates are nearly linear, N(165.9°), C (179.5°), apical NCS linear (178.1°), C (178.7°). There is a second perpendicular (90°) plane defined by N(2), N(3), N(4). The two angles involving the pyridyl and thiocyanate N centers [N(2)-Co(1)-N(3) = 144.6°(2)], [N(2)-Co(1)-N(4) = 94.8°(2)] are supportive of the distorted square pyramidal geometry.

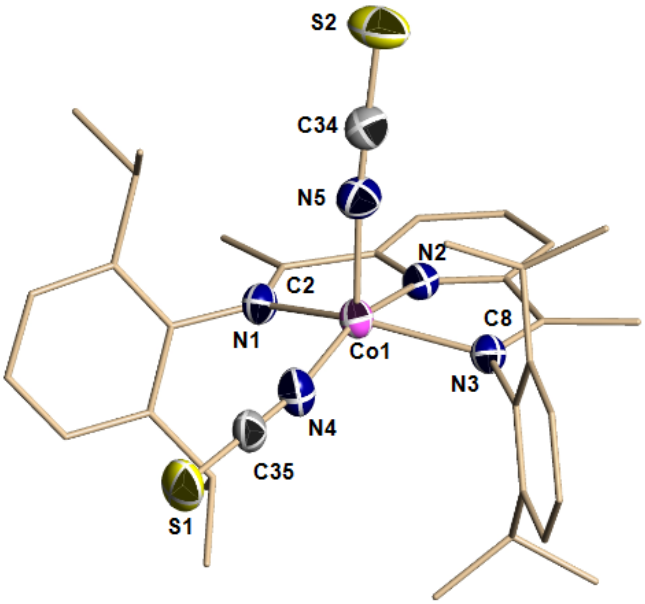

Figure 3.7 : X-ray structure of compound **3.4** with hydrogen atoms and CH_2Cl_2 omitted for clarity.

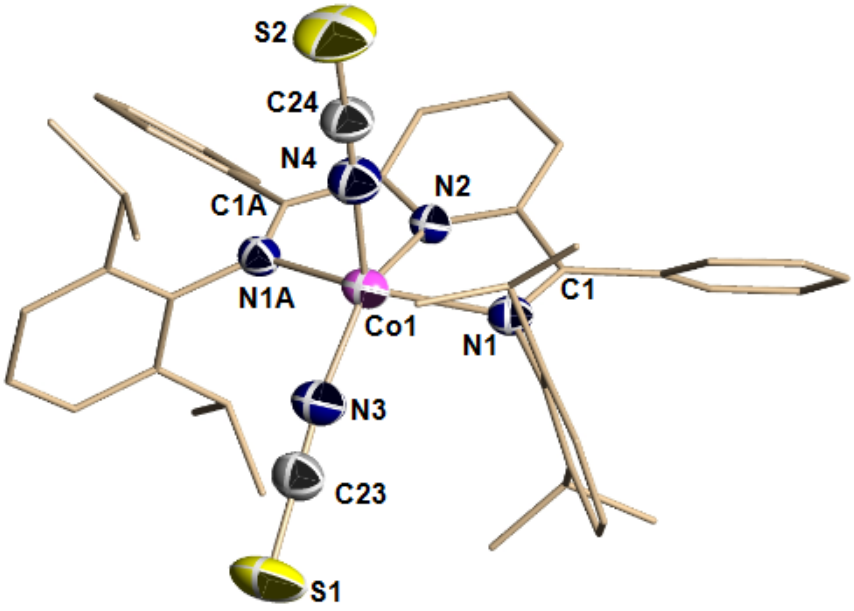

Figure 3.8 : X-ray structure of compound **3.5** with hydrogen atoms and THF omitted for clarity.

Compound **3.2** has the formula 2,6-{[$(Me_2C_6H_3)$N]CPh}$_2C_5H_3$NCo(II)$(NCS)_2$ and the relation of this compound to compound **3.1** is the same as compounds **3.4**, **3.5** (Ph for Me replacement) (Figure 3.9). As such it is not so surprising that this structure is most similar to compound **3.1**. Cobalt sits above the basal mean plane defined by N(1), N(2), N(3), N(5) by 0.477 Å. The calculated τ value is 0.19 which is closer to 0 than 1. In this compound [N(2)-Co-N(4) = 113.17°(15)] and [N(5)-Co(1)-N(2) = 139.38°(16)] deviation from ideal tbp of 120° is 6.3° and 19.38°. This suggests deviation toward square pyramidal structure.

Summary, the ligand R groups do play a role on the distortion of the metal geometry as revealed by these structures the primary effects are from the N-Ar with secondary from C-R.

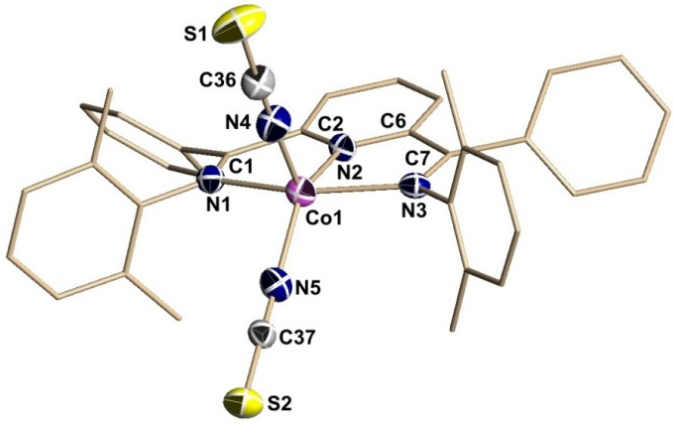

Figure 3.9 : X-ray structure of compound **3.2** with hydrogen atoms and CH_2Cl_2 omitted for clarity. Select bond lengths and angles are given in Tables 3.2 and 3.3.

In analogous fashion to **3.2** and **3.5**, ligands **2.4** and **2.5** were reacted with $CoBr_2$ for 18 hours (Scheme 3.3). The resulting green powders were isolated in 73% (**3.6**) and 88% (**3.7**) yield. The molecular structure of these compounds were confirmed through single crystal X-ray analysis as summarized in Tables 3.5, 3.6, and 3.7, and Figure 3.10 and 3.11.

Scheme 3.3

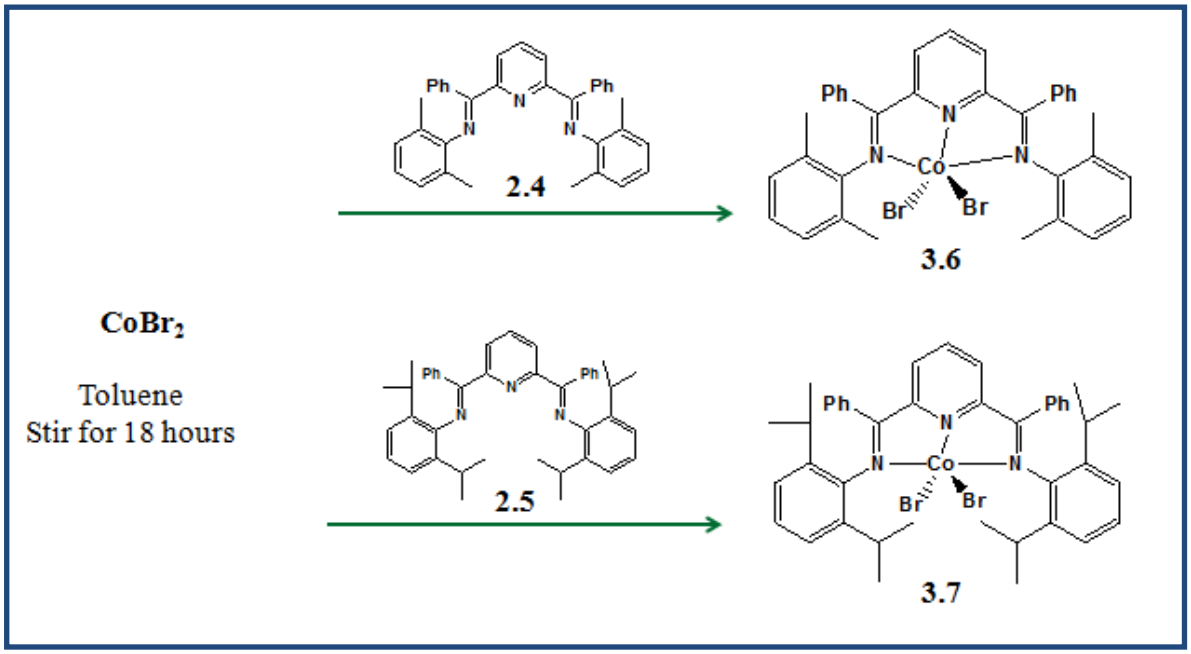

Compound **3.7** has the formula 2,6-{[($iPr_2C_6H_3$)N]CPh}$_2C_5H_3$NCo(II)$(Br)_2$ (Figure 3.10). The 2,6-diisopropylphenyl substituents on the coordinated imine nitrogen centers lie orthogonal to the basal plane of the complex and their orientation is very similar to compound **3.5.** In this compound the calculated τ value would use the two angles of [N(2)-Co(1)-Br(2) = 151.83°(15)] and [N(3)-Co(1)-N(1) = 143.72°(18)] to give a value of 0.135. The two angles involving the pyridyl and bromide, [N(2)-Co(1)-Br(1) = 92.72°(15)] and [N(2)-Co(1)-Br(2) = 151.83°(15)] supportive of the distorted square pyramidal geometry.

Compound **3.6** has the formula 2,6-{[($Me_2C_6H_3$)N]CPh}$_2C_5H_3$NCo(II)$(Br)_2$ (Figure 3.11). In this compound the calculated τ parameter of [N(2)-Co(1)-Br(2)] as the largest angle 161.30°(11) and the next larger of the remaining three angles [N(3)-Co(1)-N(1) = 141.51°(15)], obtain a τ = 0.329. While closer to 0 than 1, for a true square pyramidal species this value should be 0. In this compound [N(2)-Co-Br(1) = 90.79°(11)] and [Br(2)-Co(1)-N(2) = 161.30°(11)]. These two angles differ from the square pyramidal value by only

by 0.79, 18.7 degrees. As a result this compound **3.6** is best described as distorted square pyramidal geometry in which the coordinated nitrogen atoms from the chelate ligand and bromide form the base. The second bromide ligand lies in the apical position.

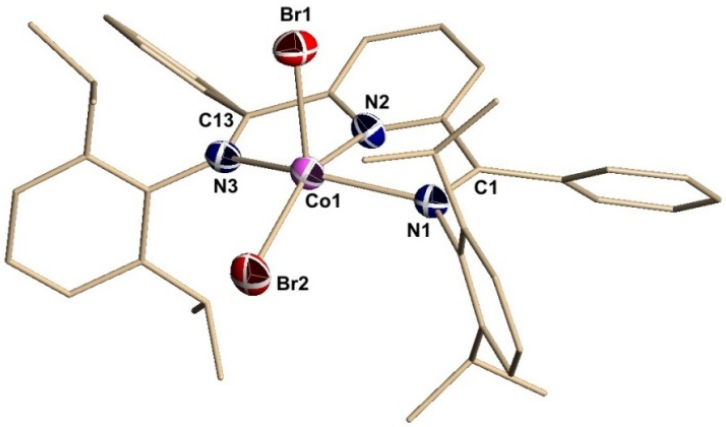

Figure 3.10 : Structure of compound **3.7** with hydrogen atoms and chlorobenzene omitted for clarity. Select bond lengths and angles are given in Tables 3.6 and 3.7.

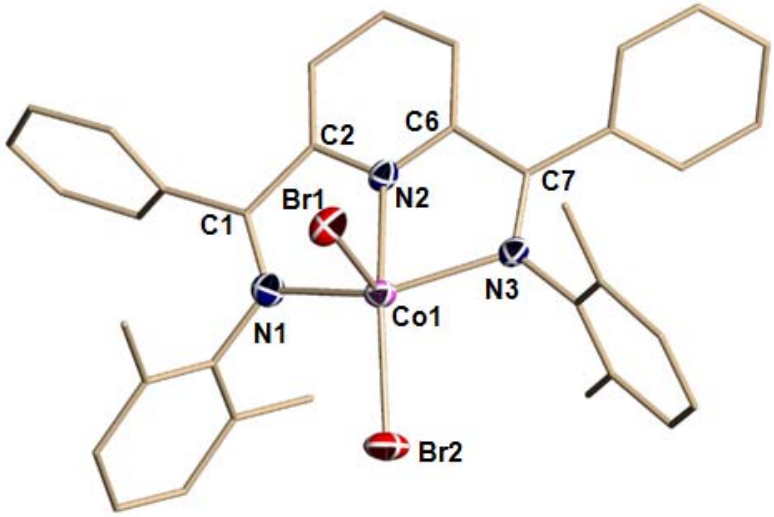

Figure 3.11 : Structure of compound **3.6** with hydrogen atoms and CH_2Cl_2 omitted for clarity. Select bond lengths and angles are given in Tables 3.6 and 3.7.

Reaction of $Co(SCN)_2$ with ligands **2.7**, shown in Scheme 3.4, directly yielded the Co complexes of this ligand as green powders **3.8** (68%). The molecular structure of this compound was confirmed through single crystal X-ray analysis as summarized in Tables 3.7, 3.8, and 3.9, and Figure 3.11.

Compound **3.8** has the formula 2,6-(2-pyridyl)$_2$C$_5$H$_3$NCo(II)(SCN)$_2$ (Figure 3.12). In this compound the calculated τ value of [N(2)#1-Co(1)-N(2)= 153.94°(6)], [N(1)-Co(1)-N(3) = 127.79°(4)], obtain a $\tau = 0.435$, and the [N(1)-Co(1)-N(3) = 127.79°(4)], and [N(1)-Co(1)-N(3)#1 = 127.79°(4)]. These two angles differ from the trigonal bipyramidal value by only by 7.79 degree. As a result this compound **3.8** is best described as distorted trigonal bipyramidal geometry.

Scheme 3.4

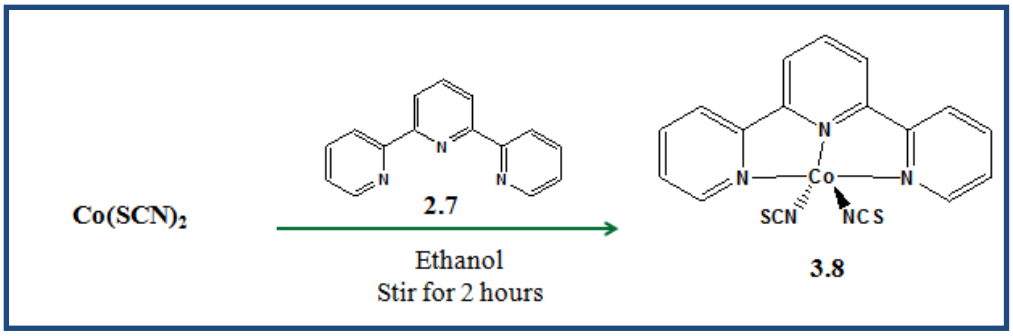

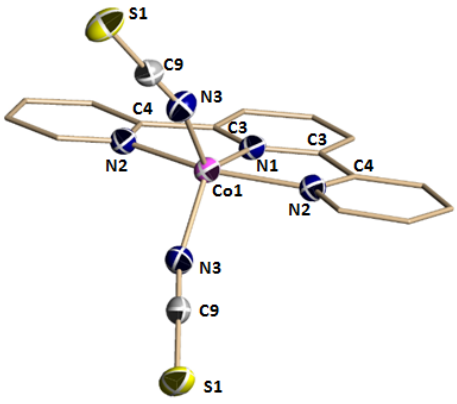

Figure 3.12: Structure of compound **3.8** with hydrogen atoms omitted for clarity. Select bond lengths and angles are given in Tables 3.8 and 3.9.

[3.3] Magnetic Measurement

The magnetic susceptibility measurements were obtained using a Quantum Design SQUID magnetometer MPMS-XL7 operating between 1.8 and 300 K for dc-applied fields ranging from −7 to 7 T. Direct current (dc) susceptibility measurements were performed on freshly filtered crushed polycrystalline sample**,** wrapped in a polyfilm membrane. Sample preparation was carried out rapidly in order to avoid any solvent loss.

Magnetic Measurement for Compound 3.3, 3.1, and 3.7:

Dc susceptibility measurement was carried out under a dc field of 1000 Oe in the 2.5-300 K temperature range (Figure 3.13, 3.14, and 3.15). At room temperature, the χT product is 2.6, 3.7, and 3.4 cm^3.K/mol for compound **3.3**, **3.1**, and **3.7** respectively which is higher than the expected theoretical spin-only value of 1.88 cm^3.K/mol for a non-interacting HS Co^{II} ion ($S = 3/2$, $g = 2$), which could be due to spin-orbit coupling.

When the temperature is lowered, the χT remain roughly constant up to 50 K and then decreases rapidly to reach 1.6, 2.5, and 2.2 cm^3.K/mol for compound **3.3**, **3.1**, and **3.7** respectively at 2.5 K which is indicative of a presence of antiferromagnetic interaction between the spin carriers.

Magnetization measurements were performed between 1.8-9.8 K between 0-4 T (Figure 3.16, 3.17, and 3.18). The *M* vs. *H* data below 9.8 K reveal a rapid increase of the magnetization at low magnetic fields. At higher fields, *M* increases linearly without clear saturation to reach 2.10, 2..5, and 2.6 μ_B for compound **3.3**, **3.1**, and **3.7** at 1.8 K and under 4 T. This high-field variation and the non-superposition on a single master-curve of the *M vs*.

H/T data suggests the presence of a significant magnetic anisotropy and/or low lying excited states in these systems.

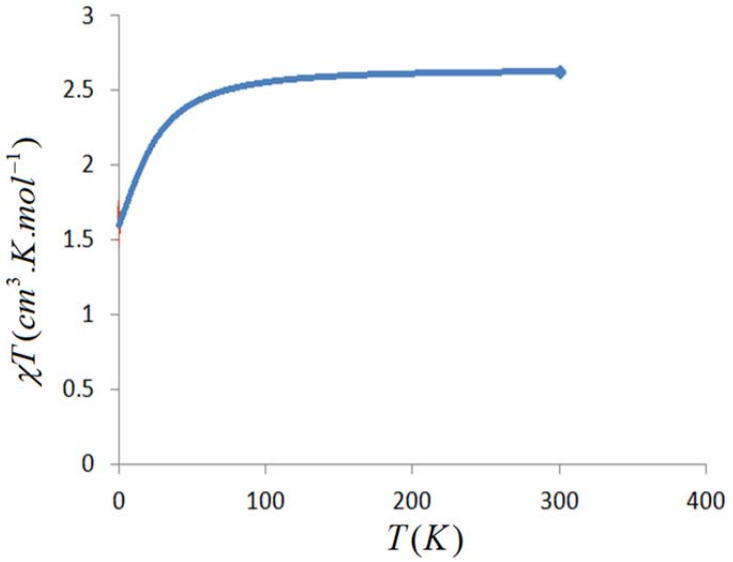

Figure 3.13: Temperature dependence of the χT product at 1000 Oe (with χ being the molar susceptibility per mononuclear complex defined as M/H) for compound **3.3**.

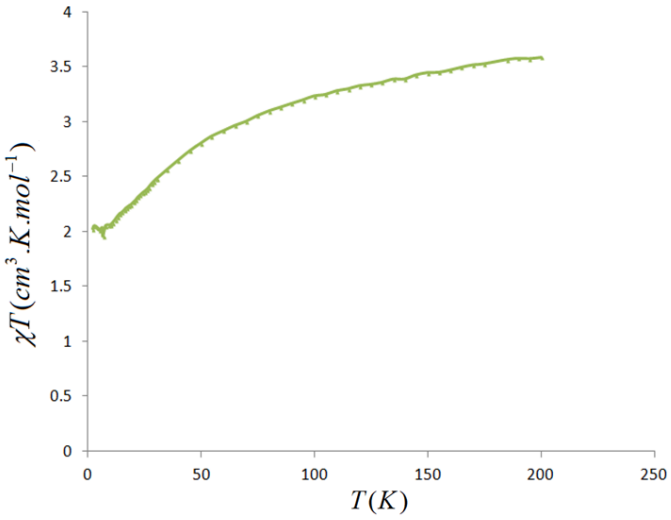

Figure 3.14: Temperature dependence of the χT product at 1000 Oe (with χ being the molar susceptibility per mononuclear complex defined as M/H) for compound **3.1**.

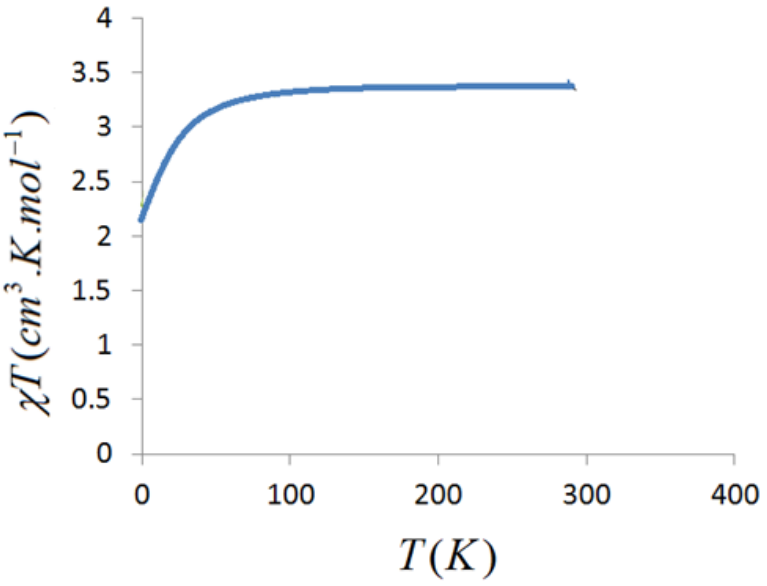

Figure 3.15: Temperature dependence of the χT product at 1000 Oe (with χ being the molar susceptibility per mononuclear complex defined as M/H) for compound **3.7**.

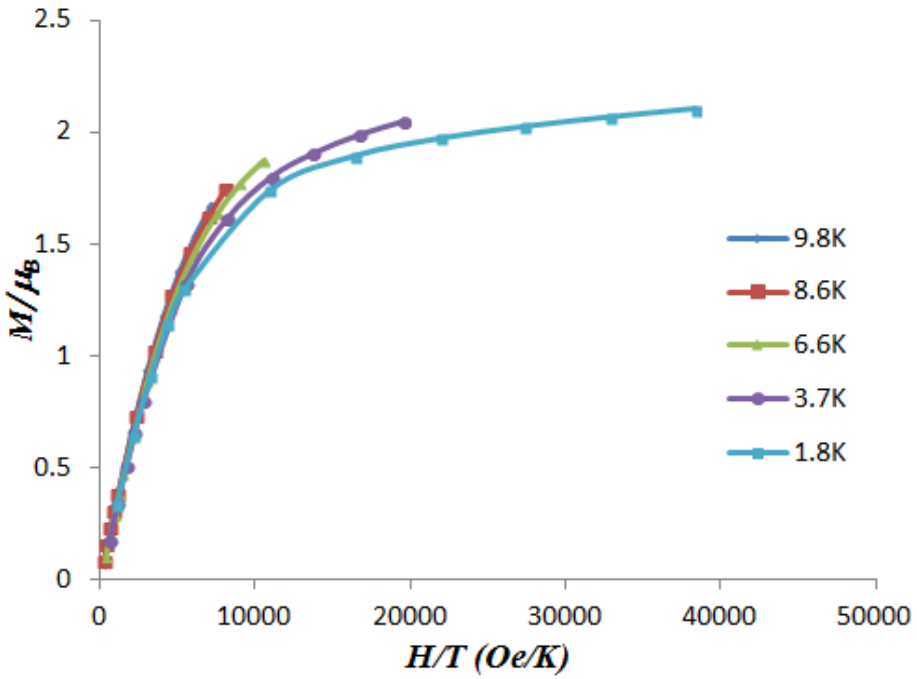

Figure 3.16. Selected curves for the field dependence of the magnetization, M, at indicated temperatures for compound **3.3.**

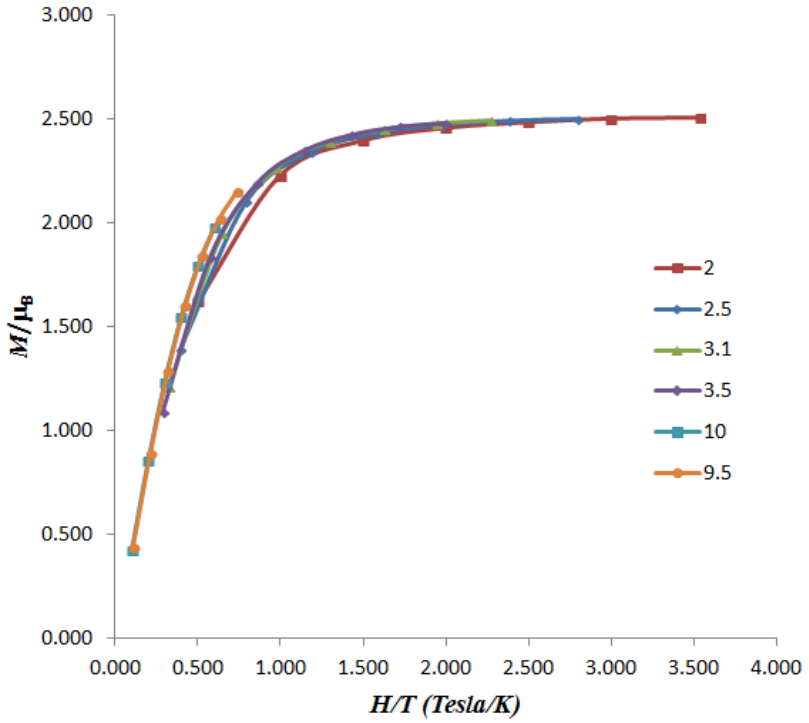

Figure 3.17. Selected curves for the field dependence of the magnetization, *M*, at indicated temperatures for compound **3.1.**

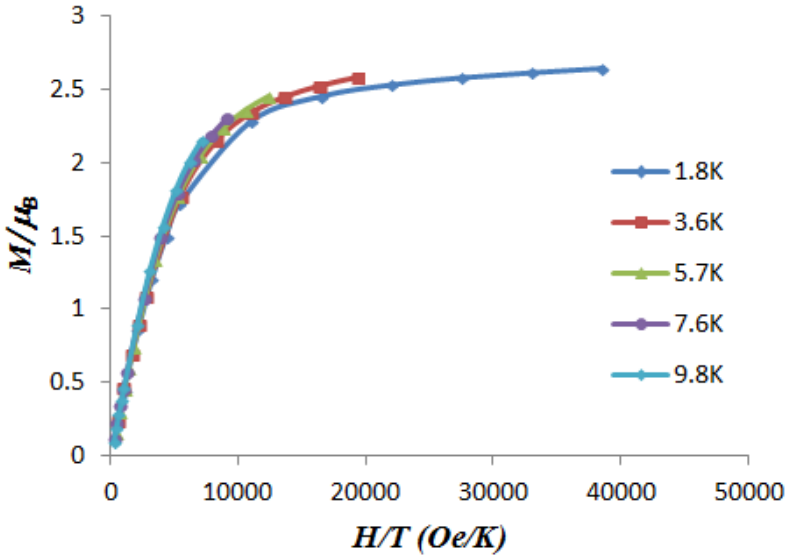

Figure 3.18. Selected curves for the field dependence of the magnetization, *M*, at indicated temperatures for compound **3.7**.

[3.4] Cobalt Complex Experimental

General Methods. Reactions were performed under lab atmosphere, with the exception of ligand synthesis, which was performed using standard Schlenk techniques under a N_2 atmosphere. Cobalt(II) thiocyanate was purchased from Strem Chemicals and used as received. All other chemicals were purchased from Aldrich and used without further purification. Compounds **2.2**, **2.3, 2.4, 2.5** and **2.6** were synthesized according to literature procedures[49,51]. Elemental analyses were performed by Midwest Microlab LLC.

(3.1) $Co(SCN)_2$-2,6-Bis[1-(2,6-dimethylphenylimino)ethyl]pyridine: $Co(SCN)_2$ powder (45 mg, 0.256 mmol) was added to a clear yellow solution of **2.2** (100 mg, 0.270 mmol) in 6 mL of toluene. The reaction mixture was allowed to stir for 14 hours, gradually becoming opaque olive green. Solution was then held at - 20^{o}C overnight, over which time a pale olive green precipitate formed. Solution was filtered, washed with 5 x 2 mL hexanes, and allowed to dry under vacuum. A opaque olive green powder was isolated in 70% yield. Brown plate-like crystals suitable for X-ray analysis were grown by diffusion of saturated CH_2Cl_2 solution in hexanes, and storing at -20^{o}C for several days. Elemental analysis calculated (%) for $[C_{27}H_{27}CoN_5S_2][CH_2Cl_2]_{0.8}$: Calcd. C 54.51, H 4.71, N 11.43, found C 54.05, H 4.59 , N 12.42.

(3.2) $Co(SCN)_2$-2,6-Bis{1-[(2,6-dimethylphenyl)imino]-benzyl}pyridine: $Co(SCN)_2$ powder (30 mg, 0.171 mmol) was added to a clear yellow solution of **2.4** (100 mg, 0.203 mmol) in 6 mL of toluene. The reaction mixture was allowed to stir for 14 hours, gradually becoming opaque olive green. Solution was then held at -20^{o}C overnight, over which time a pale olive green precipitate formed. Solution was filtered, washed with 5 x 2 mL hexanes, and allowed to dry under vacuum. A pale olive green powder was isolated in 96% yield.

Green needle-like crystals suitable for X-ray analysis were grown by diffusion of saturated CH_2Cl_2 solution in hexanes, and storing at - 20°C for several days. Elemental analysis calculated (%) for crystals grown in CH_2Cl_2 : $[C_{37}H_{31}CoN_5S_2]_3[CH_2Cl_2]_2$: Calcd. C 62.37, H 4.49, N 9.65, found C 62.01, H 4.45, N 10.27.

(3.3)Co(SCN)$_2$-2,6-Bis{1-[(2,5-ditertbutylphenyl)imino]-benzyl}pyridine: $Co(SCN)_2$ powder (22 mg, 0.125 mmol) was added to a clear yellow solution of **2.6** (100 mg, 0.139 mmol) in 6 mL of toluene. The reaction mixture was allowed to stir for 14 hours, gradually becoming brown. Solution was then held at -20°C overnight, over which time a brown precipitate formed. Solution was filtered, washed with 5 x 2 mL hexanes, and allowed to dry under vacuum. A brown powder was isolated in 69% yield. Orange block-like crystals suitable for X-ray analysis were grown by diffusion of saturated CH_2Cl_2 solution in hexanes, and storing at -20°C for several days. Elemental analysis calculated (%) for $[C_{49}H_{55}CoN_5S_2][CH_2Cl_2]_{0.7}$: Calcd. C 66.58, H 6.34, N 7.81, found C 66.60 , H 6.06, N 8.46.

(3.4) Co(SCN)$_2$-2,6-Bis{1-[(2,6-diisopropylphenyl)imino]-ethyl}pyridine:[74] $Co(SCN)_2$ powder (99 mg, 0.567 mmol) was added to a clear yellow solution of **2.3** (300 mg, 0.623 mmol) in 5 mL of toluene. The reaction mixture was sealed and allowed to stir for 6 h. A color change from translucent yellow to translucent green was observed after a few hours of stirring. The solution was then held at -20˚C for 48 h, to produce a light green precipitate. The reaction mixture was filtered; the solid was washed with 3 x 5 mL hexanes, and dried under vacuum. The product, a light green powder, was isolated in 97% yield. Crystals suitable for X-ray analysis were grown by slow vapor diffusion of hexanes into a moderately saturated solution of CH_2Cl_2 at -20˚C for several days. Elemental analysis performed on crystals grown by layering hexanes into a saturated solution of CH_2Cl_2.

Elemental Analysis for $[C_{35}H_{43}CoN_5S_2]_3[CH_2Cl_2]$: Calcd. C 61.94, H 6.42, N 10.22, Found C 62.28 H 6.40, N 10.25.

(3.5) Co(SCN)$_2$-2,6-Bis{1-[(2,6-diisopropylphenyl)imino]-benzyl}pyridi[74] $Co(NCS)_2$ powder (56 mg, 0.320 mmol) was added to a clear yellow solution of **2.5** (200 mg, 0.330 mmol) in 5 mL of toluene. The reaction mixture was sealed and allowed to stir for 6 h. A color change from translucent yellow to translucent brown was observed after a few hours of stirring. The solution was then held at -20˚C for 48 h, to produce a light brown precipitate. The reaction mixture was filtered, the solid was washed with 3 x 5 mL hexanes, and dried under vacuum. The product, a light brown powder, was isolated in 95% yield. Crystals suitable for X-ray analysis were grown by slow vapor diffusion of hexanes into a saturated solution of THF at - 20˚C for several days. Elemental analysis for $[C_{45}H_{47}CoN_5S_2]$: Calcd. C 69.21, H 6.07, N 8.97, Found C 68.95, H 5.99, N 8.88.

(3.6) CoBr$_2$-2,6-Bis{1-[(2,6-dimethylphenyl)imino]-benzyl}pyridine: $CoBr_2$ powder (35 mg, 0.160 mmol) was added to a clear yellow solution of **2.4** (100 mg, 0.165 mmol) in a mixture of 2 mL toluene, and 4 mL hexanes. The reaction mixture was allowed to stir for 4 hours, gradually becoming opaque bronze. Solution was then held at -20^{o}C overnight, over which time a bronze precipitate formed. Solution was filtered, washed with 5 x 2 mL hexanes, and allowed to dry under vacuum. A fine brown powder was isolated in 73% yield. Brown needle-like crystals suitable for X-ray analysis were grown by diffusion of saturated dichloromethane solution in hexanes, and storing at -20^{o}C for several days. Elemental analysis calculated (%) for $[C_{35}H_{31}Br_2CoN_3][CH_2Cl_2]_{0.7}$: Calcd. C 57.40, H 4.37, N 5.63, found C 57.18, H 4.26, N 5.49.

[74] Ahmed M. S. Farghal, Ottawa, Canada, 2012.

(3.7) $CoBr_2$-2,6-Bis{1-[(2,6-diisopropylphenyl)imino]-benzyl}pyridine: $CoBr_2$ powder (35 mg, 0.160 mmol) was added to a clear yellow solution of **2.5** (100 mg, 0.165 mmol) in a mixture of 2 mL toluene, and 4 mL hexanes. The reaction mixture was allowed to stir for 4 hours, gradually becoming opaque bronze. Solution was then held at -20°C overnight, over which time a bronze precipitate formed. Solution was filtered, washed with 5 x 2 mL hexanes, and allowed to dry under vacuum. A fine bronze powder was isolated in 88% yield. Orange block-like crystals suitable for X-ray analysis were grown by diffusion of saturated chlorobenzene solution in hexanes, and storing at -20°C for several days. Elemental analysis calculated (%) for [$C_{43}H_{47}Br_2CoN_3$]: Calcd. C 62.63, H 5.75, N 5.10, found C 62.61, H 5.78, N 5.03.

***(3.8) $Co(SCN)_2$* (terpy):**[75-77] $Co(SCN)_2$ powder (75 mg, 428 mmol) was added to a clear solution of terpyridyl (100 mg, 0.428 mmol) in 20 mL of ethanol. The reaction mixture was refluxed for 2 hours, gradually becoming dark green. Solution was then held at -20°C overnight, over which time a dark green precipitate formed. Solution was filtered, washed with 5 x 2 mL hexanes, and allowed to dry under vacuum. A dark green powder was isolated in 68% yield. Blue block-like crystals suitable for X-ray analysis were grown by diffusion of saturated CH_2Cl_2 solution in hexanes, and storing at - 20°C for several days. Elemental analysis calculated (%) for [$C_{17}H_{11}CoN_5S_2$]: Calcd. C 50.00 , H 2.72 , N 17.15, found C 49.61 , H 2.76 , N 16.55.

---

[75] Harris, C.; Lockyer. T. N.; Martin, L.; Pate, H. R. H. *Aust. J. Chem.* **1969**, *22,* 2105.

[76] Morgan, G.; Burstall, F. H. *J. Chem. Soc.* **1937**, 1649.

[77] Hogg, R.; Wilkins, R. G. *J. Chem. Soc.* **1962**, 341.

[3.5] X-ray Crystallographic Information: Cobalt Complexes

Table 3.1. Summary of Data Collection and Crystallographic Parameters for **3.1**, **3.2**, and **3.3**.

Compound	**3.1**	**3.2**	**3.3**
Empirical formula	$C_{28}H_{29}Cl_2CoN_5S_2$	$C_{39}H_{35}Cl_4CoN_5S_2$	$C_{49}H_{55}CoN_5S_2$
Formula weight	629.51	838.57	837.03
Temperature(K)	200(2)	200(2)	200(2)
λ (Å)	0.71073	0.71073	0.71073
Crystal system	Monoclinic	Orthorhombic	Orthorhombic
Space group	P2(1)/n	Pna2(1)	Pbca
a (Å)	13.3392(3)	15.0227(3)	17.8805(7)
b (Å)	14.4970(3)	19.1952(4)	20.3571(8)
c (Å)	16.4639(4)	13.8726(3)	25.0102(10)
α (deg)	90	90	90
β (deg)	107.1960(10)	90	90
γ (deg)	90	90	90
V ($Å^3$)	3041.44(12)	4000.35(14)	9103.6(6)
Z	4	4	8
p (calc) (Mg/m3)	1.375	1.392	1.221
m (mm^{-1})	0.903	0.835	0.507
R1[a]	0.0829	0.0481	0.0999
wR2[b]	0.1687	0.094	0.1975

Table 3.2. Selected bond lengths (Å) for **3.1**, **3.2**, and **3.3**.

3.1		**3.2**		**3.3**	
Co(1)-N(5)	1.950(3)	Co(1)-N(4)	1.957(4)	Co(1)-N(4)	1.931(6)
Co(1)-N(4)	1.957(3)	Co(1)-N(5)	1.967(4)	Co(1)-N(5)	2.002(9)
Co(1)-N(2)	2.020(2)	Co(1)-N(2)	2.025(3)	Co(1)-N(2)	2.044(4)
Co(1)-N(1)	2.188(2)	Co(1)-N(3)	2.231(4)	Co(1)-N(3)	2.152(5)
Co(1)-N(3)	2.236(2)	Co(1)-N(1)	2.246(4)	Co(1)-N(1)	2.219(4)
N(1)-C(2)	1.281(4)	N(1)-C(1)	1.279(5)	N(1)-C(1)	1.287(7)
N(2)-C(3)	1.338(4)	N(2)-C(6)	1.333(5)	N(2)-C(6)	1.327(7)
N(2)-C(7)	1.340(4)	N(2)-C(2)	1.332(5)	N(2)-C(2)	1.344(7)
N(3)-C(8)	1.284(4)	N(3)-C(7)	1.280(6)	N(3)-C(7)	1.300(7)
N(4)-C(26)	1.150(4)	N(4)-C(36)	1.155(6)	N(4)-C(48)	1.146(8)
N(5)-C(27)	1.142(4)	N(5)-C(37)	1.156(5)	N(5)-C(49)	1.176(9)
C(2)-C(3)	1.497(4)	C(1)-C(2)	1.507(6)	C(1)-C(2)	1.481(8)
C(7)-C(8)	1.492(4)	C(6)-C(7)	1.506(6)	C(6)-C(7)	1.492(8)
S(1)-C(26)	1.619(4)	C(36)-S(1)	1.620(6)	S(1)-C(48)	1.608(7)
S(2)-C(27)	1.612(4)	C(37)-S(2)	1.607(5)	S(2)-C(49)	1.609(8)

Table 3.3. Selected bond angles (˚) for compounds **3.1**, **3.2**, and **3.3**.

3.1		**3.2**		**3.3**	
N(5)-Co(1)-N(4)	109.05(12)	N(4)-Co(1)-N(5)	107.42(16)	N(4)-Co(1)-N(5)	104.3(2)
N(5)-Co(1)-N(2)	137.58(11)	N(4)-Co(1)-N(2)	113.17(15)	N(4)-Co(1)-N(2)	167.7(2)
N(4)-Co(1)-N(2)	113.31(10)	N(5)-Co(1)-N(2)	139.38(16)	N(5)-Co(1)-N(2)	88.0(2)
N(5)-Co(1)-N(1)	96.74(10)	N(4)-Co(1)-N(3)	95.08(16)	N(4)-Co(1)-N(3)	101.3(2)
N(4)-Co(1)-N(1)	102.87(11)	N(5)-Co(1)-N(3)	102.59(15)	N(5)-Co(1)-N(3)	107.1(2)
N(2)-Co(1)-N(1)	76.28(9)	N(2)-Co(1)-N(3)	75.88(14)	N(2)-Co(1)-N(3)	74.67(17)
N(5)-Co(1)-N(3)	98.67(10)	N(4)-Co(1)-N(1)	99.04(16)	N(4)-Co(1)-N(1)	104.0(2)
N(4)-Co(1)-N(3)	95.91(10)	N(5)-Co(1)-N(1)	97.13(15)	N(5)-Co(1)-N(1)	96.1(2)
N(2)-Co(1)-N(3)	75.17(9)	N(2)-Co(1)-N(1)	75.33(14)	N(2)-Co(1)-N(1)	73.99(17)
N(1)-Co(1)-N(3)	150.26(9)	N(3)-Co(1)-N(1)	151.04(13)	N(3)-Co(1)-N(1)	139.9(18)
C(2)-N(1)-Co(1)	114.46(19)	C(1)-N(1)-C(20)	119.8(4)	C(1)-N(1)-Co(1)	110.0(3)
C(10)-N(1)-Co(1)	125.38(19)	C(1)-N(1)-Co(1)	113.8(3)	C(20)-N(1)-Co(1)	116.6(3)
C(3)-N(2)-Co(1)	118.71(19)	C(20)-N(1)-Co(1)	125.8(3)	C(6)-N(2)-Co(1)	120.7(4)
C(7)-N(2)-Co(1)	120.2(2)	C(6)-N(2)-Co(1)	119.9(3)	C(2)-N(2)-Co(1)	118.3(4)
C(8)-N(3)-Co(1)	114.4(2)	C(7)-N(3)-Co(1)	113.4(3)	C(7)-N(3)-Co(1)	115.8(4)
C(18)-N(3)-Co(1)	125.05(19)	C(28)-N(3)-Co(1)	128.1(3)	C(34)-N(3)-Co(1)	117.0(3)
C(26)-N(4)-Co(1)	173.4(3)	C(36)-N(4)-Co(1)	178.8(4)	C(48)-N(4)-Co(1)	167.4(6)
C(27)-N(5)-Co(1)	175.0(3)	C(37)-N(5)-Co(1)	168.5(4)	C(49)-N(5)-Co(1)	166.2(6)
N(4)-C(26)-S(1)	178.5(4)	N(4)-C(36)-S(1)	178.5(5)	N(4)-C(48)-S(1)	177.7(6)
N(5)-C(27)-S(2)	178.3(3)	N(5)-C(37)-S(2)	179.4(5)	N(5)-C(49)-S(2)	178.9(7)

Table 3.5. Summary of Data Collection and Crystallographic Parameters for **3.6** and **3.7.**

Compound	**3.6**	**3.7**
Empirical formula	C_{37} H_{35} Br_2 Cl_4 Co N_3	$C_{52}H_{54.50}Br_2Cl_{1.50}CoN_3$
Formula weight	882.23	993.41
Temperature(K)	200(2)	200(2)
λ (Å)	0.71073	0.71073
Crystal system	Triclinic	Monoclinic
Space group	P-1	C2/c
a (Å)	8.6323(9)	55.973(3)
b (Å)	13.1122(12)	10.5504(5)
c (Å)	17.8710(16)	19.2842(10)
α (deg)	108.709(4)	90
β (deg)	94.081(4)	109.029(2)
γ (deg)	94.516(4)	90
V (Å3)	1900.0(3)	10765.6(9)
Z	2	8
p (calc) (Mg/m3)	1.542	1.226
m (mm-1)	2.866	1.911
R1a	0.1584	0.107
wR2b	0.1539	0.2303

Table 3.6. Selected bond lengths (Å) for **3.6 and 3.7.**

3.6		**3.7**	
Co(1)-N(2)	2.048(4)	Co(1)-N(2)	2.032(5)
Co(1)-N(3)	2.197(4)	Co(1)-N(3)	2.222(5)
Co(1)-N(1)	2.193(4)	Co(1)-N(1)	2.281(5)
Co(1)-Br(2)	2.3829(9)	Co(1)-Br(2)	2.3576(10)
Co(1)-Br(1)	2.4616(8)	Co(1)-Br(1)	2.4354(11)
N(1)-C(1)	1.290(6)	N(1)-C(1)	1.290(8)
N(2)-C(6)	1.329(6)	N(2)-C(8)	1.330(8)
N(2)-C(2)	1.354(6)	N(3)-C(13)	1.287(8)
N(3)-C(7)	1.290(6)	N(2)-C(12)	1.337(8)
C(1)-C(2)	1.487(7)	C(1)-C(2)	1.503(9)
C(6)-C(7)	1.493(7)	C(12)-C(13)	1.501(9)

Table 3.7. Selected bond angels (˚) for compounds **3.6 and 3.7.**

3.6		**3.7**	
N(2)-Co(1)-N(3)	74.44(15)	N(2)-Co(1)-N(3)	74.92(19)
N(2)-Co(1)-N(1)	74.14(16)	N(2)-Co(1)-N(1)	73.93(19)
N(3)-Co(1)-N(1)	141.51(15)	N(3)-Co(1)-N(1)	143.72(18)
N(2)-Co(1)-Br(2)	161.30(11)	N(2)-Co(1)-Br(2)	151.83(15)
N(3)-Co(1)-Br(2)	104.14(11)	N(3)-Co(1)-Br(2)	100.32(13)
N(1)-Co(1)-Br(2)	98.62(12)	N(1)-Co(1)-Br(2)	98.39(13)
N(2)-Co(1)-Br(1)	90.79(11)	N(2)-Co(1)-Br(1)	92.72(15)
N(3)-Co(1)-Br(1)	99.43(10)	N(3)-Co(1)-Br(1)	98.13(13)
N(1)-Co(1)-Br(1)	102.67(12)	N(1)-Co(1)-Br(1)	101.45(13)
Br(2)-Co(1)-Br(1)	107.73(3)	Br(2)-Co(1)-Br(1)	115.45(4)
C(1)-N(1)-Co(1)	114.6(3)	C(1)-N(1)-C(20)	119.8(5)
C(20)-N(1)-Co(1)	124.2(3)	C(1)-N(1)-Co(1)	112.9(4)
C(6)-N(2)-Co(1)	120.3(3)	C(20)-N(1)-Co(1)	127.2(4)
C(2)-N(2)-Co(1)	119.6(3)	C(8)-N(2)-Co(1)	119.9(4)
C(7)-N(3)-Co(1)	115.4(3)	C(12)-N(2)-Co(1)	117.1(4)
C(28)-N(3)-Co(1)	121.8(3)	C(13)-N(3)-Co(1)	114.2(4)

Table 3.8. Summary of Data Collection and Crystallographic Parameters for **3.8** and **3.9**.

Compound	**3.8**
Empirical formula	$C_{17}H_{11}CoN_5S_2$
Formula weight	408.36
Temperature(K)	200(2)
λ (Å)	0.71073
Crystal system	Monoclinic
Space group	C2/c
a (Å)	13.7450(3)
b (Å)	9.4051(2)
c (Å)	14.4231(4)
α (deg)	90
β (deg)	110.9300(10)
γ (deg)	90
V (Å3)	1741.49(7)
Z	4
p (calc) (Mg/m3)	1.558
m (mm-1)	1.234
R1a	0.0254
wR2b	0.0682

Table 3.9. Selected bond lengths (Å) for **3.8** and **3.9**.

3.8	
Co(1)-N(3)	1.9775(11)
Co(1)-N(3)#1	1.9776(11)
Co(1)-N(1)	2.0272(14)
Co(1)-N(2)#1	2.1460(11)
Co(1)-N(2)	2.1460(11)
S(1)-C(9)	1.6211(13)
N(1)-C(3)#1	1.3424(14)
N(1)-C(3)	1.3424(14)
N(2)-C(8)	1.3400(18)
N(2)-C(4)	1.3452(17)
N(3)-C(9)	1.1547(18)

Table 3.10. Selected bond angles (˚) for compounds **3.8** and **3.9**.

3.8	
N(3)-Co(1)-N(3)#1	104.42(7)
N(3)-Co(1)-N(1)	127.79(4)
N(3)#1-Co(1)-N(1)	127.79(4)
N(3)-Co(1)-N(2)#1	93.41(4)
N(3)#1-Co(1)-N(2)#1	102.53(4)
N(1)-Co(1)-N(2)#1	76.97(3)
N(3)-Co(1)-N(2)	102.53(4)
N(3)#1-Co(1)-N(2)	93.41(4)
N(1)-Co(1)-N(2)	76.97(3)
N(2)#1-Co(1)-N(2	153.94(6)
N(3)-C(9)-S(1)	179.02(13)

[3.6] Infra-Red for Cobalt Complex

Infra-Red spectra were collected using a Cary 630 FT-IR spectrometer.

Table 3.11 : Infra-Red for compounds **3.1**, **3.2**, **3.3**, and **3.8**.

bond	**3.1**	**3.2**	**3.3**	**3.8**
C=N imine stretch	1585,1665	1461,1584	1492,1571	-
-N=C=S stretch	2055	2063	2054	2060
-N=C=S stretch	2115	2083	2074	2061

Table 3.12 : Infra-Red for compounds **3.6** and **3.7**.

Bond	**3.6**	**3.7**
C=N imine, stretch	1570	1597, 1623

Chapter 4

Synthesis and Characterization of Fe (II) Metal Center with the Bis(imino)pyridine Ligand Framework.

[4.1] Introduction

As outlined in Chapter 3, first example of a mononuclear transition metal based on single-molecule magnet was reported by Long and Chang in 2009. In this case, SMM behavior was observed for $[(tpaMes)Fe]^-$ with trigonal pyramidal coordination geometry (Figure 4.1).[78] The d-orbital splitting shown in Figure 4.1 was used to rationalize the observation of slow magnetic relaxation behavior for these mononuclear Fe(II) complexes.[79,80] This configuration allows for spin-orbit coupling and magnetic anisotropy.

Motivated by our success with Co(II), we looked at the Fe(II) with one less electron, and employed bis(imino)pyridine ligands to synthesize mononuclear Fe(II) complexes with the same geometry as cobalt complexes. Much like Co(II), Fe(II) has an inherently high magnetic anisotropy among the first row transition metals. The orbital configuration for high-spin Fe(II) in ideal trigonal bipyramidal and square pyramidal coordination geometries is shown in Figure 4.2. Orbital configuration for high-spin Fe(II) center ($S = 2$) reveals spin-

[78] Harman, W. H.; Harris, T. D.; Freedman, D. E.; Fong, H.; Chang, A; Rinehart, J. D.; Ozarowski, A.; Sougrati, M. T.; Grandjean, F.; Long, G. J.; Long, J. R.; Chang, C. J. *J. Am. Chem. Soc*. **2010**, *132*, 18115.

[79] Freedman, D. E.; Harman, W. H.; Harris, T. D.; Long, G. J.; Chang, C. J.; Long, J. R. *J. Am. Chem. Soc.* **2010**, *132*, 1224.

[80] Weismann, D.; Sun, Y.; Lan, Y.; Wolmershauser, G.; Powell, A. K.; Sitzmann, H. *Chem.Eur. J.* **2011**, *17*, 4700.

orbit coupling in ideal tbp and sp coordination geometries (orbital contribution possible), thereby Fe(II) complexes in these geometries could exhibit slow magnetic relaxation behavior.

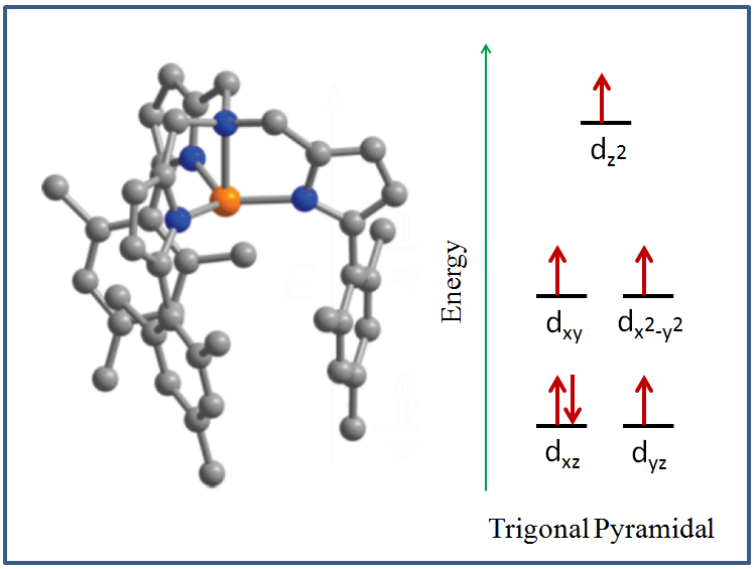

Figure 4.1: Structure of the trigonal pyramidal complex $[(tpaMes)Fe]^-$ (left), Splitting of the 3d orbital energies for a high-spin Fe(II) center in a trigonal pyramidal ligand field (right).

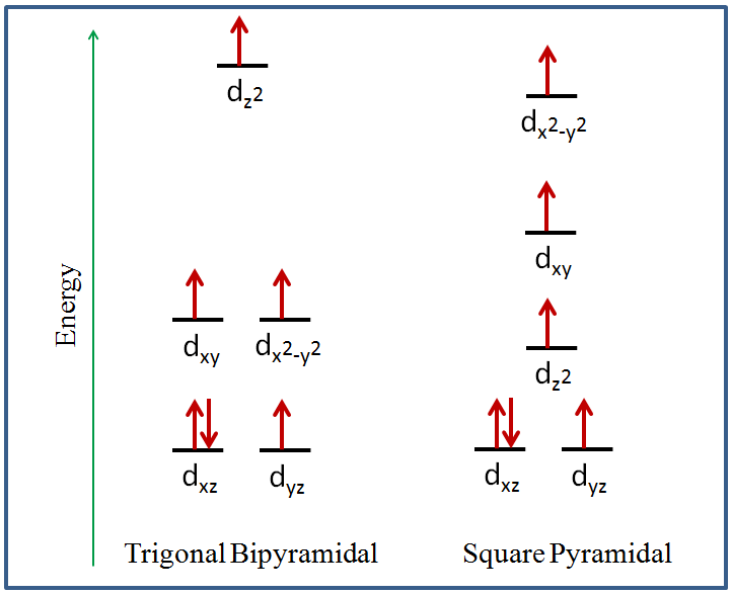

Figure 4.2: Splitting of the 3d orbital energies for a high-spin Fe(II) center in a trigonal bipyramidal (left) and square pyramidal (right) ligand field.

We employed the bis(imino)pyridine ligand to synthesis high-spin Fe(II) complexes based on single-molecule magnet, and magnetic anisotropy was enhanced by controlling the geometry of these five coordinate species through modification of bis(imino)pyridine ligand. Similar to Co(II) complexes, we employed bromide, isothiocyanide, and cyanide ligands, that occupy a single coordination site, to make flexibility in metal environment.

[4.2] Results and Discussion: Synthesis, Characterization

Fe(II) Complexes of the bis(imino)pyridine ligand frame were prepared by the addition of ligand **2.3**, **2.5** and **2.4** to a solution of $Fe(SCN)_2$ (Scheme 4.1), which provided **4.1**, **4.2** and **4.3** as dark green solids in 56%, 54%, and 72% yields respectively. The molecular structure of these compounds were confirmed through single crystal X-ray analysis as summarized in Tables 4.1, 4.2 and 4.3 and Figure 4.3, 4.5, and 4.6.

Scheme 4.1

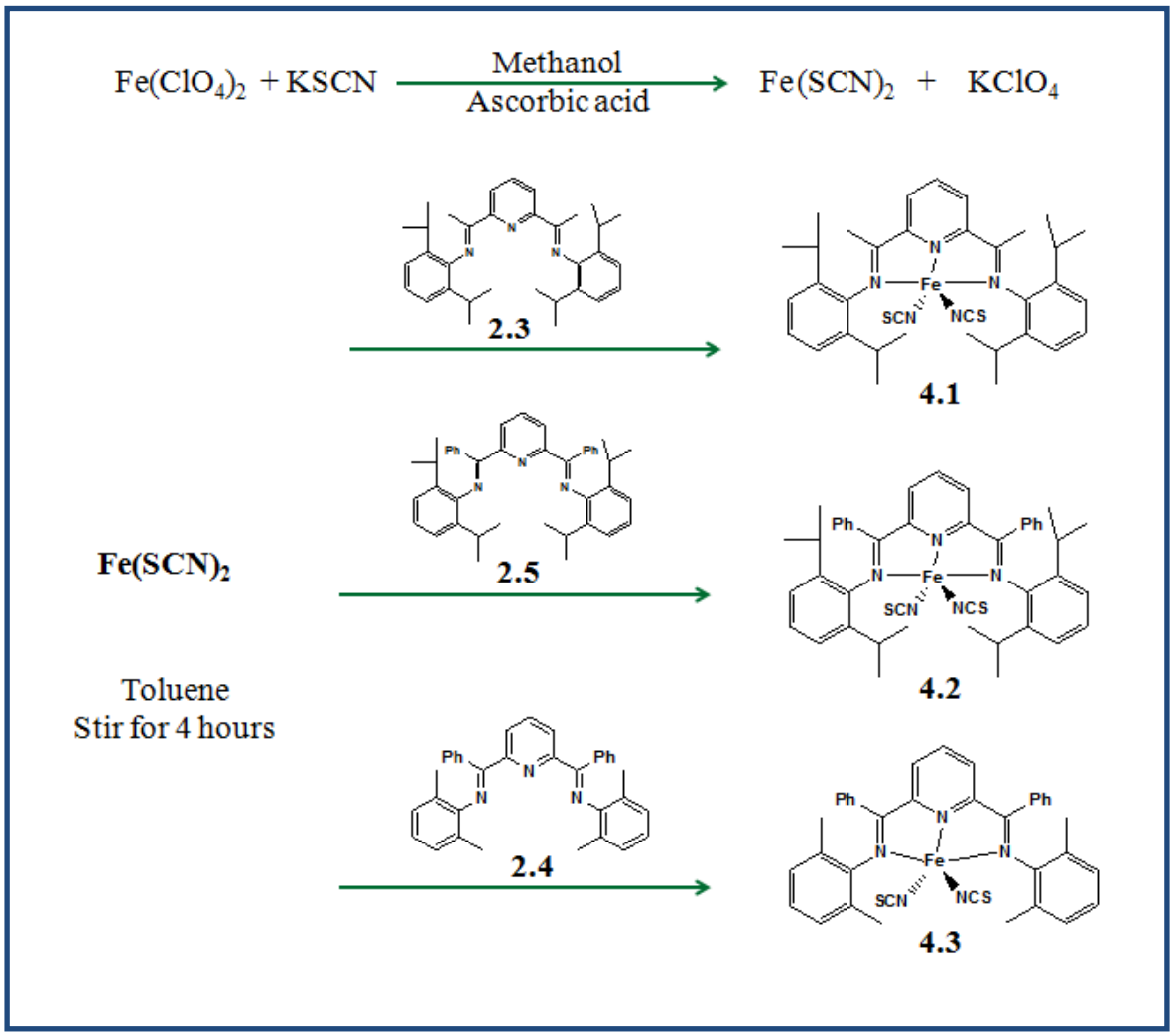

Compound **4.1** has the formula 2,6-{[($iPr_2C_6H_3$)N]CMe}$_2C_5H_3NFe(II)(NCS)_2$ and coordination geometry looks more like compound **3.4** with the iron in a distorted square pyramidal environment **(**Figure 4.3**)**. The basal mean plane can be defined by N(1), N(2), N(3), N(4). This plane also contains the ligand framework and the pyridine ring carbons (Figure 4.4). The thiocyanates are close to linear with the angles around N (171.4°, 171.5°) and C(176.9°, 178.7°). In this compound, the calculated τ parameter is 0.14 and a perpendicular molecular plane can be defined by N(2), N(4), N(5), and [N(2)-Fe(1)-N(4) = 150.8°(3)] and [N(2)-Fe(1)-N(5) = 106.1°(3)]. These are the angles to define distorted square pyramidal geometry.

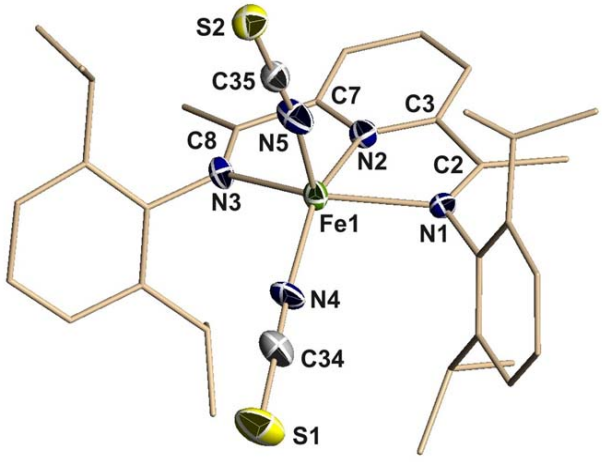

Figure 4.3 : Structure of compound **4.1** with hydrogen atoms and CH_2Cl_2 omitted for clarity. Select bond lengths and angles are given in Tables 4.2 and 4.3.

Compound **4.2** has the formula 2,6-{[($iPr_2C_6H_3$)N]CPh}$_2C_5H_3NFe(II)(NCS)_2$ (Figure 4.5). Again, it appears that the ligand plane forms the basal plane for a pseudo-square planar Fe complex. The pyridyl group lies in the plane. The diisopropylaryl substituents on the coordinated imine nitrogen centers lie orthogonal to the basal plane of the complex. The two thiocyanates are linear with angles for the nitrogen and carbon centers [FeN(4)C(44)

=165.9°], [S(2)C(44)N(4) = 179.5°], apical NCS is linear (178.1°), [S(1)C(45)N(5) = 178.7°]. The symmetry of this complex displays a second perpendicular (90°) plane defined by N(2), N(5), N(4). In this compound the calculated τ parameter is 0.054. The two angles involving the pyridyl and thiocyanate N centers [N(2)-Fe(1)-N(5) = 92.53°(7)], [N(2)-Fe(1)-N(4) = 148.69°(8)] are supportive of the distorted square pyramidal geometry.

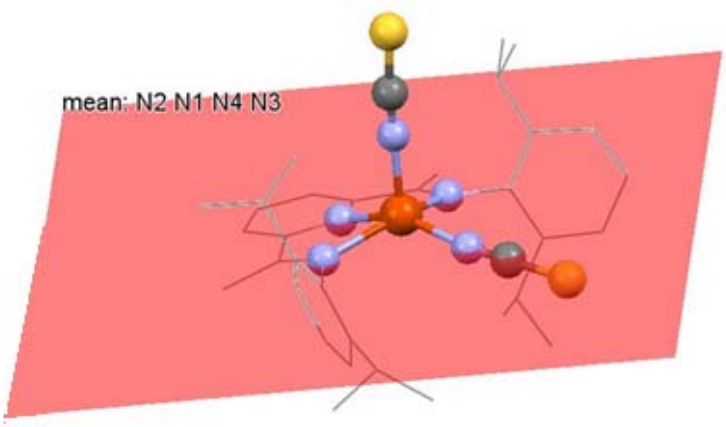

Figure 4.4 : Structure of compound **4.1** with hydrogen atoms and CH_2Cl_2 omitted for clarity. Plane contains the ligand framework and the pyridine ring carbons.

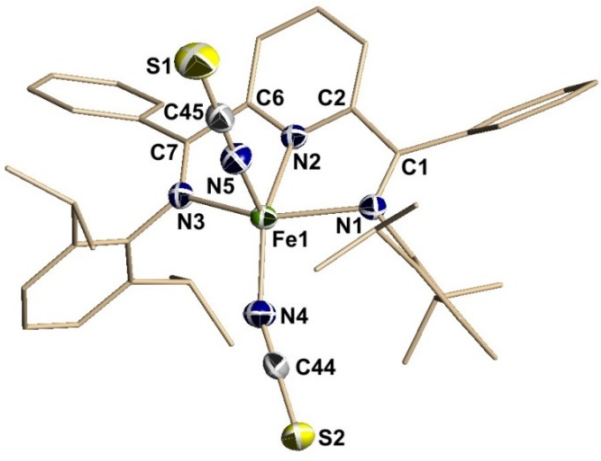

Figure 4.5 : Structure of compound **4.2** with hydrogen atoms omitted for clarity. Select bond lengths and angles are given in Tables 4.2 and 4.3.

Compound **4.3** has the formula 2,6-{[($Me_2C_6H_3$)N]CPh}$_2$$C_5H_3$NFe(II)($NCS)_2$ (Figure 4.6). In this compound the calculated τ parameter using [N(1)-Fe(1)-N(3) = 146.56° (14)] and [N(5)-Fe(1)-N(2)=142.16°(14)], is 0.07. Analysis of [N(2)-Fe-N(4) = 115.32° (13)] and [N(5)-Fe(1)-N(2) = 142.16°(14)] deviate from ideal tbp of 120° by 4.68° and 22.16°. Clearly this indicates the deviation it toward square pyramidal structure.

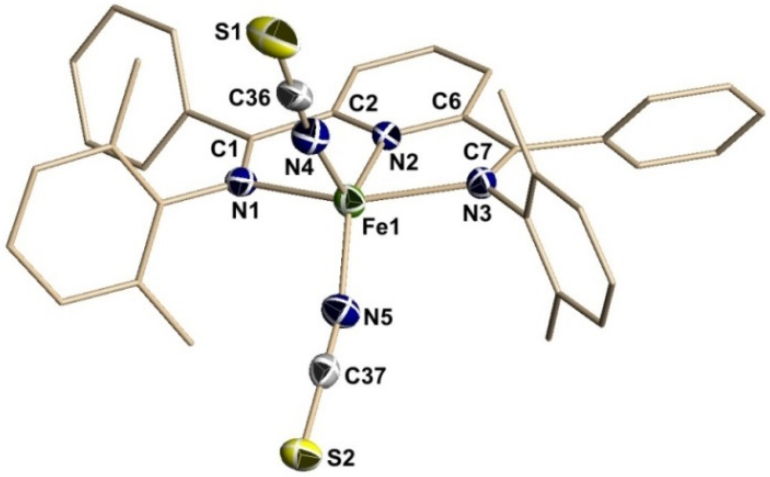

Figure 4.6 : Structure of compound **4.3** with hydrogen atoms and $CHCl_3$ omitted for clarity. Select bond lengths and angles are given in Tables 4.2 and 4.3.

Scheme 4.2

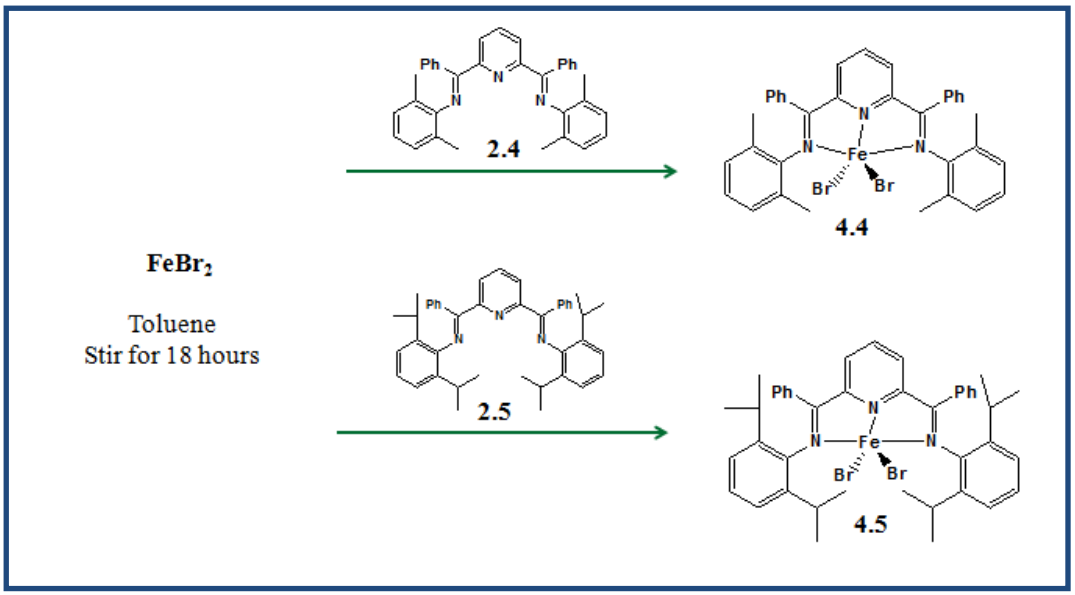

Reaction of $FeBr_2$ with ligands **2.4** and **2.5**, shown in Scheme 4.2, directly yielded the Fe complexes of these ligands as green powders **4.4** (93%) and **4.5** (78%). The molecular structures of these compounds were confirmed through single crystal X-ray analysis as summarized in Tables 4.4, 4.5 and 4.6, and Figure 4.7 and 4.8.

Compound **4.4** has the formula 2,6-{[$(Me_2C_6H_3)$N]CPh}$_2C_6H_3$NFe(II)$(Br)_2$ (Figure 4.7). The calculated τ parameter is 0.065 and analysis of [N2-Fe(1)-N1 = 73.80°(9)] and [N(5)-Co(1)-N(2) = 147.47°(7)] show large deviation from ideal square pyramidal of 90° and180° (16.2° and 32.53°). These are the angles to define distorted square pyramidal geometry.

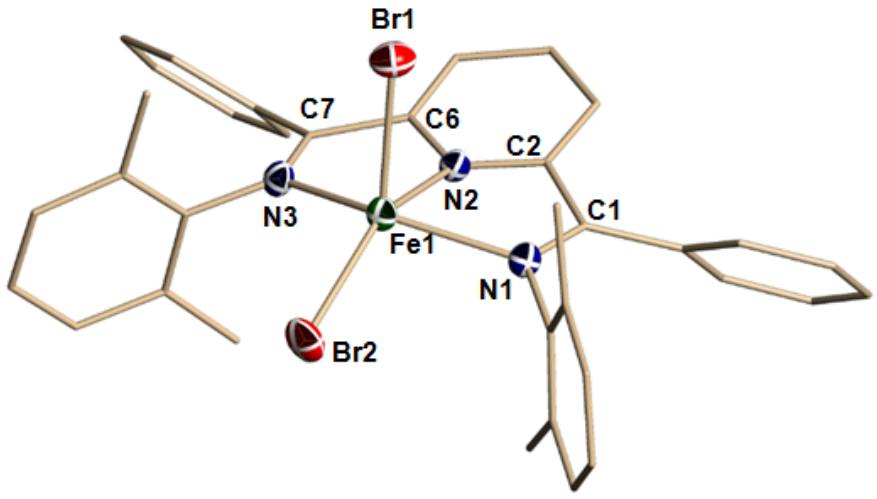

Figure 4.7 : Structure of compound **4.4** with hydrogen atoms and CH_2Cl_2 omitted for clarity. Select bond lengths and angles are given in Tables 4.5 and 4.6.

Compound **4.5** has the formula 2,6-{[$(iPr_2C_6H_3)$N]CPh}$_2C_6H_3$NFe(II)$(Br)_2$ (Figure 4.8). In this compound the calculated τ value is 0.134. The two angles involving the pyridyl and bromide [N(2)-Fe(1)-Br(1)=92.75°(13)] and [N(2)-Fe(1)-Br(2)=150.63°(14)] supportive of the distorted square pyramidal geometry.

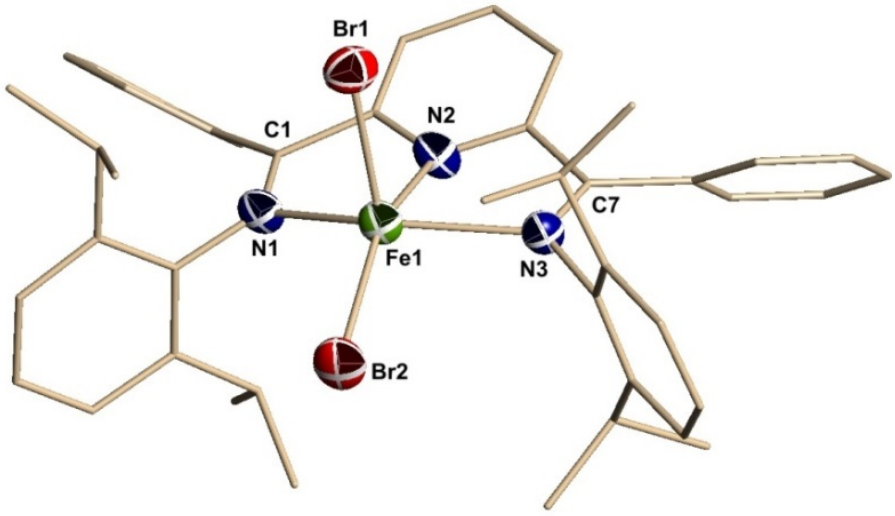

Figure 4.8 : Structure of compound **4.5** with hydrogen atoms and chlorobenzene omitted for clarity. Select bond lengths and angles are given in Tables 4.5 and 4.6.

[4.3] Magnetic Measurement

The magnetic susceptibility measurements were obtained using a Quantum Design SQUID magnetometer MPMS-XL7 operating between 1.8 and 300 K for dc-applied fields ranging from −7 to 7 T. Direct current (dc) susceptibility measurements were performed on freshly filtered crushed polycrystalline sample, wrapped in a polyethylene membrane. Sample preparation was carried out rapidly in order to avoid any solvent loss.

Magnetic measurement for Compound 4.2:

The magnetization data were collected at 100 K to check for ferromagnetic impurities that were absent in all samples. A diamagnetic correction was applied for the sample holder and Pascal constants were used for the diamagnetic correction of the sample (Figure 4.9).

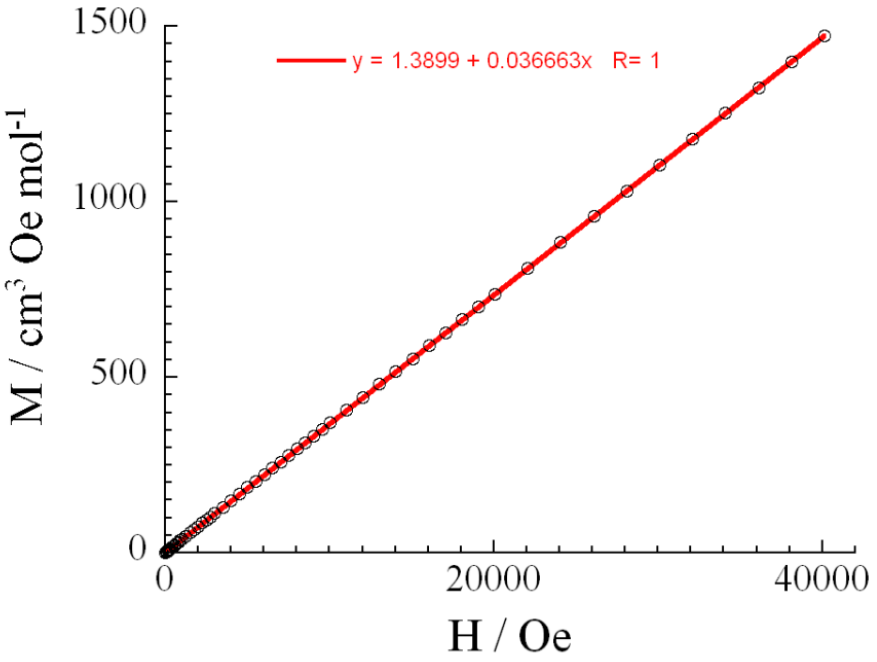

Figure 4.9: Magnetization data were collected at 100 K. The observed straight line is indicative of absence of any impurities for compound **4.2.**

Dc susceptibility measurement was carried out under a dc field of 1000 Oe in the 2.5-300 K temperature range (Figure 4.10). At room temperature, the χT product is 3.77 cm^3K/mol which is slightly higher than the expected theoretical spin-only value of 3 cm^3K/mol for a non-interacting HS Fe^{II} ion ($S = 2$, $g = 2$).

When the temperature is lowered, the χT remain roughly constant up to 50 K and then decreases rapidly to reach 2.54 cm^3.K/mol at 2.5 K which is indicative of a presence of antiferromagnetic interaction between the spin carriers.

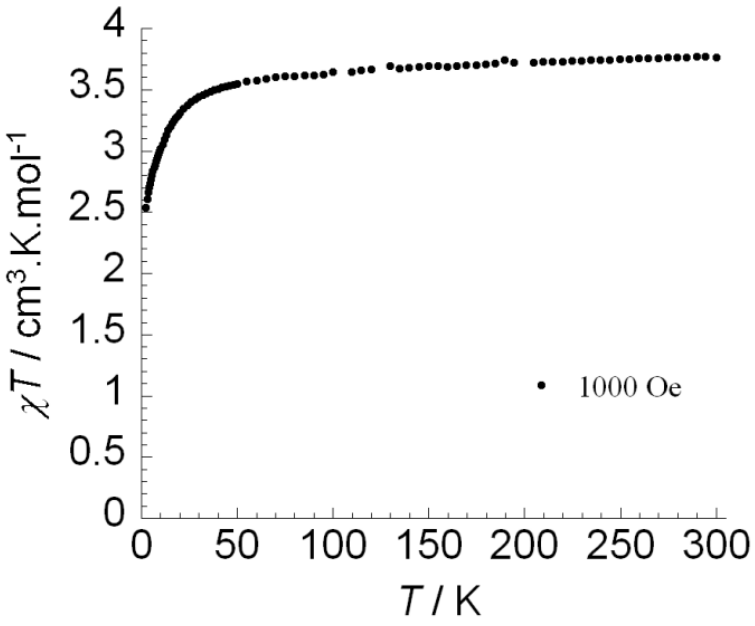

Figure 4.10: Temperature dependence of the χT product at 1000 Oe (with χ being the molar susceptibility per mononuclear complex defined as M/H) for compound **4.2**.

Magnetization measurements were performed between 2.5-8 K between 0-7 T (Figure 4.11 and 4.12). The *M* vs. *H* data below 8 K reveal a rapid increase of the magnetization at low magnetic fields. At higher fields, *M* increases linearly without clear saturation to reach 3.10 μ_B at 2.5 K and under 7 T. This high-field variation and the non-superposition on a single master-curve of the *M vs. H/T* data (Figures 4.12) suggests the presence of a significant magnetic anisotropy and/or low lying excited states in these systems. The ac susceptibility in zero dc field shows a complete absence of out-of-phase component above 2.5 K.

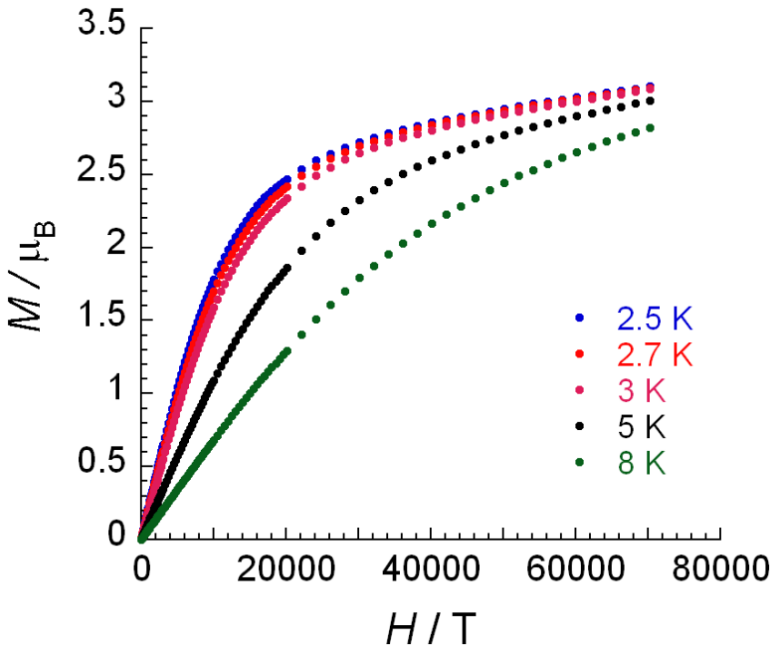

Figure 4.11. Field dependence of the magnetization, *M*, at indicated temperatures for compound **4.2.**

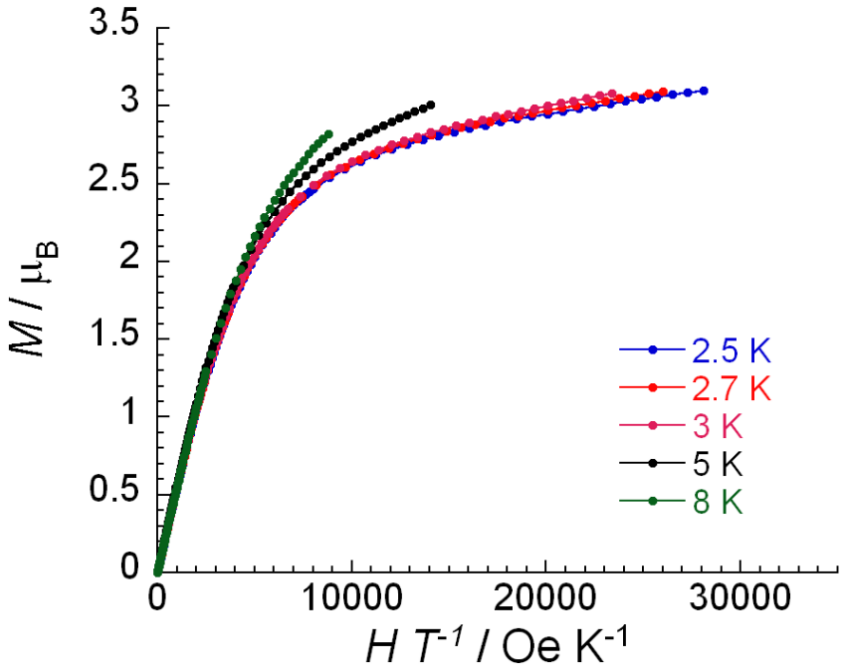

Figure 4.12. *M* vs *H*/*T* plot measured at 2.5, 2.7, 3, 5, and 8 K for compound **4.2.**

Magnetic measurement for Compound for compound 4.1, 4.4, and 4.5:

Dc susceptibility measurement was carried out under a dc field of 1000 Oe in the 2.5-300 K temperature range (Figure 4.13, 4.14, and 4.15). At room temperature, the χT product is 3.61, 4.0, and 4.32 cm^3.K/mol for compound 4.1, 4.4, and 4.5 which is slightly higher than the expected theoretical spin-only value of 3 cm^3.K/mol for a non-interacting HS Fe^{II} ion ($S = 2$, $g = 2$).

When the temperature is lowered, the χT remain roughly constant up to 50 K and then decreases rapidly to reach 2.1, 2.5, and 2.9 cm^3.K/mol for compound 4.1, 4.4, and 4.5 at 2.5 K which is indicative of a presence of antiferromagnetic interaction between the spin carriers.

Magnetization measurements were performed between 1.8-9.8 K between 0-4 T (Figure 4.16, 4.17, and 4.18). The M vs. H data below 9.8 K reveal a rapid increase of the magnetization at low magnetic fields. At higher fields, M increases linearly without clear saturation to reach 3.10, 3.4. and 3.2 μ_B for compound 4.1, 4.4, 4.5 at 1.8K and under 4 T.

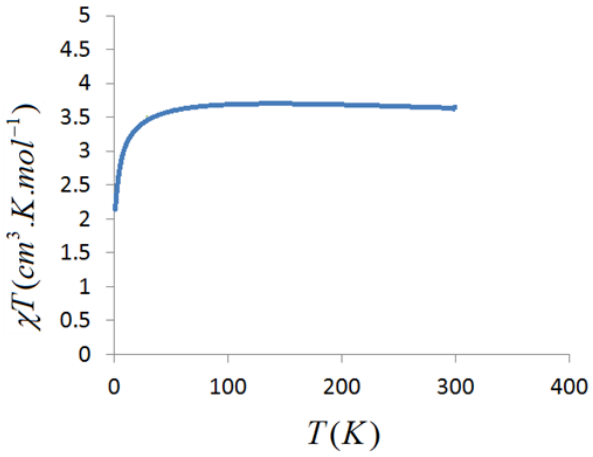

Figure 4.13: Temperature dependence of the χT product at 1000 Oe (with χ being the molar susceptibility per mononuclear complex defined as M/H) for compound **4.1.**

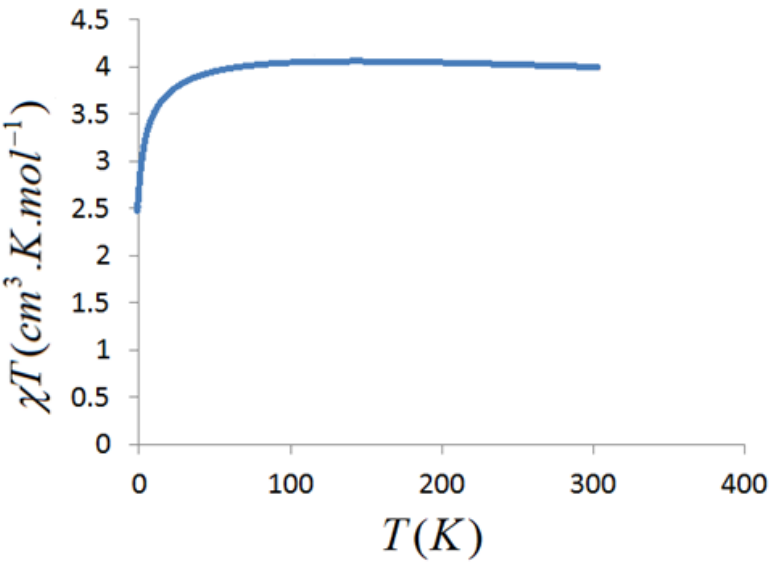

Figure 4.14: Temperature dependence of the χT product at 1000 Oe (with χ being the molar susceptibility per mononuclear complex defined as M/H) for compound **4.4.**

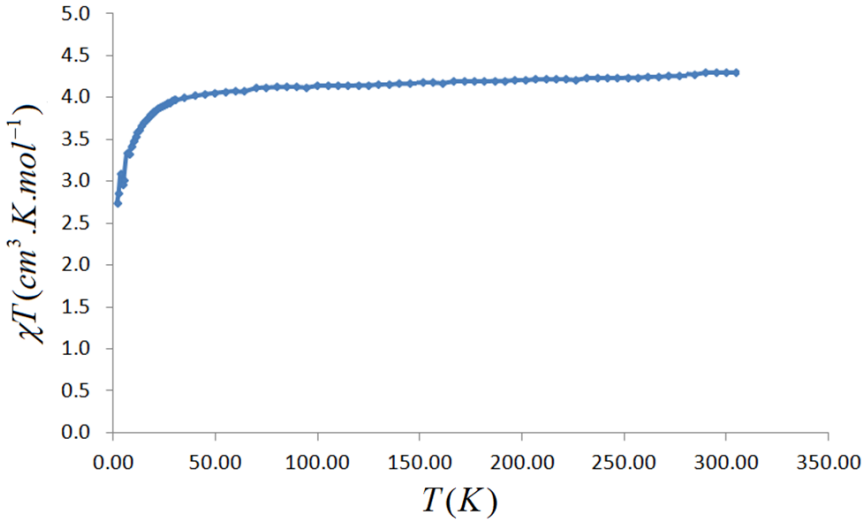

Figure 4.15: Temperature dependence of the χT product at 1000 Oe (with χ being the molar susceptibility per mononuclear complex defined as M/H) for compound **4.5.**

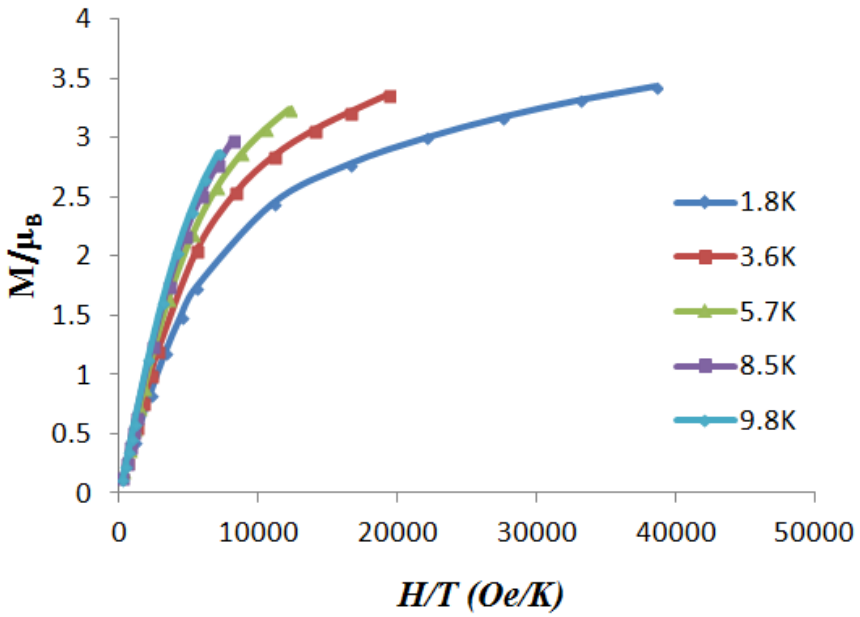

Figure 4.16. Selected curves for the field dependence of the magnetization, *M*, at indicated temperatures for compound **4.1.**

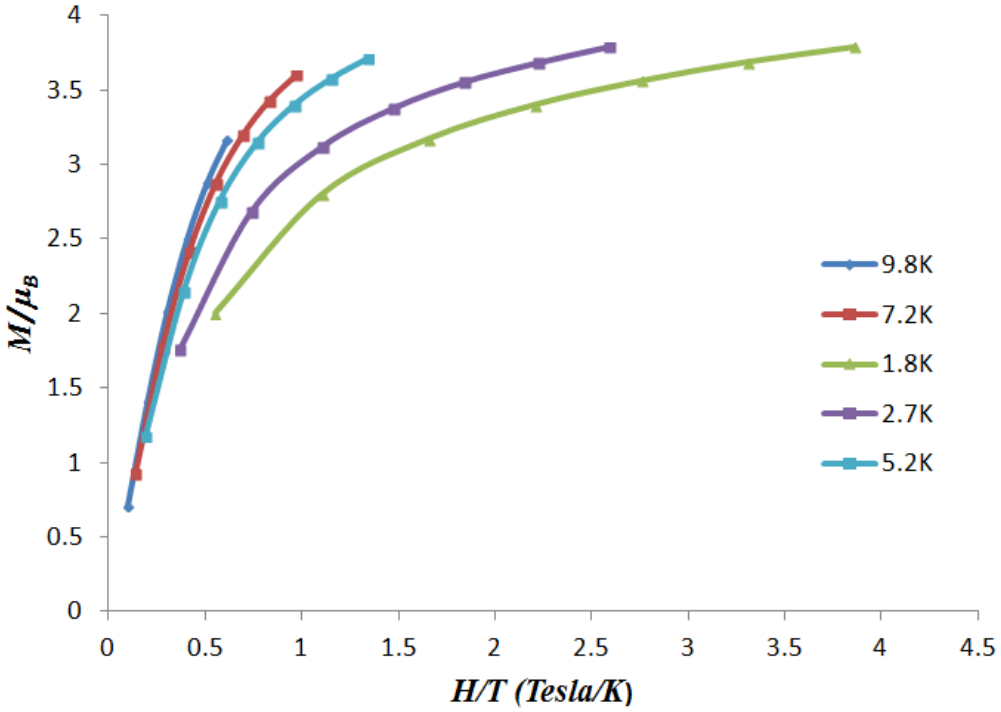

Figure 4.17. Field dependence of the magnetization, *M*, at indicated temperatures for compound **4.4.**

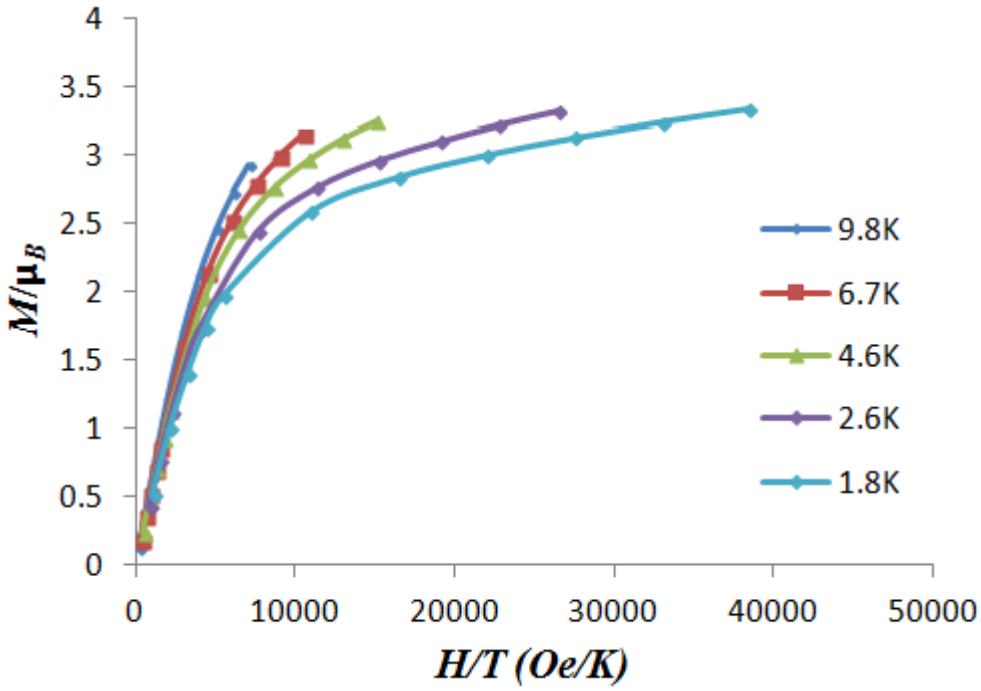

Figure 4.18. Selected curves for the field dependence of the magnetization, *M*, at indicated temperatures for compound **4.5.**

[4.4] Iron Complex Experimental

General Methods. Reactions were performed under a lab atmosphere, with the exception of ligand synthesis, which was performed using standard Schlenk techniques under a N_2 atmosphere. Iron(II) bromide was purchased from Strem Chemicals and used as received. All other chemicals were purchased from Aldrich and used without further purification. Compounds **2.4**, **2.6** and **2.7** were synthesized according to literature procedures.[49,51] Elemental analyses were performed by Midwest Microlab LLC.

(4.1) $Fe(SCN)_2$-2,6-Bis{1-[(2,6-diisopropylphenyl)imino]-methyll}pyridine: A solution of KSCN (40 mg, 0.4 mmol) in 1 mL of MeOH was added dropwise to a solution of $Fe(ClO_4)_2.6H_2O$ (52 mg, 0.2 mmol) and a small amount of ascorbic acid in 1 mL of MeOH. Instantly a precipitate of $KClO_4$ was formed and after 2-3 minutes filtered off. The colorless solution of $Fe(NCS)_2$ was added to a clear yellow solution of **2.3** (100 mg, 0.2 mmol) in 15 mL of toluene. The reaction mixture turned dark green and was allowed to stir for 2 h. During this time a white precipitate formed. White solid was removed by filtration yielded a green solution. The solvent was removed under vacuum to give a pale green solid and was washed with 5 x 2 mL hexane. The product was obtained as a brown powder. Yield: 56.3%. Brown block-like crystals suitable for X-ray analysis were grown from a saturated CH_2Cl_2 solution with diffusion of hexane. Elemental analysis calculated (%) for $[C_{35}H_{43}FeN_5S_2][CH_2Cl_2]_{0.3}$: C 62.42, H 6.47, N 10.31 , found C 62.17, H 6.73, N 9.74.

***(4.2)$Fe(SCN)_2$-2,6-Bis{1-[(2,6-diisopropylphenyl)imino]-benzyl}pyridine*:**

Method A: A solution of KSCN (28 mg, 0.28 mmol) in 1 mL of MeOH was added dropwise to a solution of $Fe(ClO_4)_2.6H_2O$ (36.3 mg, 0.14 mmol) and a small amount of ascorbic acid in 1 mL of MeOH. Instantly a precipitate of $KClO_4$ was formed and after 2-3

minutes filtered off. The resulting colorless solution of $Fe(NCS)_2$ was added to a clear yellow solution of **2.5** (85 mg, 0.14 mmol) in 15 mL of toluene. The reaction mixture turned green and was allowed to stir for 2 h. During this time a dark green precipitate formed. The mixture was filtered, and the precipitate was washed with 5 x 2 mL hexane, and allowed to dry under vacuum. The product was obtained as a dark green powder. Yield: 54%. Green needle-like crystals suitable for X-ray analysis were grown by from a saturated solution of chloroform with hexane diffusion**.** Elemental analysis calculated (%) for $[C_{45}H_{47}FeN_5S_2]$: C 69.48, H 6.09, N 9.00, found C 69.33 , H 6.07, N 8.91.

Method B: KSCN powder (3.5 mg, 0.036 mmol) was added to a green solution of **4.5** (15 mg, 0.018 mmol) in 5 mL toluene. The reaction mixture was allowed to stir for 4 hours, During this time a white precipitate formed. White solid was removed by filtration to yield a green solution. The solvent was removed under vacuum to give a dark green solid and was washed with 5 x 2 mL hexane. A green powder was isolated in 37% yield. Green rod-like crystals suitable for X-ray analysis were grown from a saturated dichloromethane solution with diffusion of hexane. The unit cell of these crystals was identical to **4.2**.

***(4.3) $Fe(SCN)_2$-2,6-Bis{1-[(2,6-dimethylphenyl)imino]-benzyl}pyridine*:** A solution of KSCN (70 mg, 0.72 mmol) in 1 mL of MeOH was added dropwise to a solution of $Fe(ClO_4)_2.6H_2O$ (100 mg, 0.39 mmol) and a small amount of ascorbic acid in 1 mL of MeOH. Instantly a precipitate of $KClO_4$ was formed and after 2-3 minutes filtered off. The colorless solution of $Fe(NCS)_2$ was added to a clear yellow solution of **2.4** (190 mg, 0.38 mmol) in 15 mL of toluene. The reaction mixture turned green and was allowed to stir for 2 h. During this time a purple precipitate formed. The reaction solvent was evaporated and the precipitate was dissolved in chloroform and a quantity of a purple solid was removed by

filtration yielded a green solution. The solvent was removed under vacuum to give a dark green solid and was washed with 5 x 2 mL hexane. The product was obtained as a green powder. Yield: 72%. Blue block-like crystals suitable for X-ray analysis were grown from a saturated chloroform solution with diffusion of hexane. Elemental analysis calculated (%) for $[C_{37}H_{31}FeN_5S_2][CH_2Cl_2]_{0.2}$: C 65.45, H 4.64, N 10.26, found C 65.66 , H 4.75, N 10.25 .

(4.4) $FeBr_2$-2,6-Bis{1-[(2,6-dimethylphenyl)imino]-benzyl}pyridine: $FeBr_2$ powder (42 mg, 0.19 mmol) was added to a clear yellow solution of **2.4** (100 mg, 0.2 mmol) in 6 mL of toluene. The reaction mixture was allowed to stir for 18 hours, gradually becoming dark green. Solution was then held at -20^{o}C overnight, over which time a dark green precipitate formed. Solution was filtered, washed with 5 x 2 mL hexanes, and allowed to dry under vacuum. A dark green powder was isolated in 93% yield. Blue plate-like crystals suitable for X-ray analysis were grown by from a saturated dichloromethane solution by diffusion of hexanes, and storing at -20^{o}C for several days. Elemental analysis calculated (%) for $[C_{35}H_{31}Br_2FeN_3][CH_2Cl_2]_{0.3}$: C 59.27, H 4.41, N 5.92, found C 57.71 , H 4.80 , N 4.67.

(4.5) $FeBr_2$-2,6-Bis{1-[(2,6-diisopropylphenyl)imino]-benzyl}pyridine: $FeBr_2$ powder (34 mg, 0.160 mmol) was added to a clear yellow solution of **2.5** (100 mg, 0.165 mmol) in 6 mL of toluene. The reaction mixture was allowed to stir for 4 hours, gradually becoming opaque dark green. Solution was then held at -20^{o}C overnight, over which time a dark green precipitate formed. Solution was filtered, washed with 5 x 2 mL hexanes, and allowed to dry under vacuum. A dark green powder was isolated in 78% yield. Green needle-like crystals suitable for X-ray analysis were grown from saturated chlorobenzene solution by diffusion of hexanes, and storing at -20^{o}C for several days. Elemental analysis

calculated (%) for [$C_{43}H_{47}Br_2FeN_3$]: C 62.87, H 5.77, N 5.12, found C 62.48, H 5.79, N 4.94.

[4.5] X-ray Crystallographic Information: Iron Complexes

Table 4.1 : Summary of Data Collection and Crystallographic Parameters for **4.1**, **4.2**, and **4.3.**

Compound	**4.1**	4.2	**4.3**
Empirical formula	$C_{72.75}H_{92.50}Cl_{5.50}Fe_2N_{10}S_4$	$C_{45}H_{47}FeN_5S_2$	$C_{39}H_{33}Cl_6FeN_5S_2$
Formula weight	1541.98	777.85	904.37
Temperature(K)	200(2)	200(2)	200(2)
λ (Å)	0.71073	0.71073	0.71073
Crystal system	Triclinic	Monoclinic	Orthorhombic
Space group	P-1	P2(1)/c	Pna2(1)
a (Å)	11.7171(6)	13.7220(10)	15.0660(3)
b (Å)	17.4910(9)	19.7428(15)	19.9928(3)
c (Å)	20.0331(11)	16.0273(12)	13.8840(3)
α (deg)	88.209(3)	90	90
β (deg)	87.348(3)	99.412(5)	90
γ (deg)	81.919(3)	90	90
V (Å3)	4059.3(4)	4283.5(6)	4182.02(14)
Z	2	4	4
p (calc) (Mg/m3)	1.262	1.206	1.436
m (mm-1)	0.686	0.485	0.879
R1a	0.1575	0.0628	0.0538
wR2b	0.3309	0.0889	0.1022

Table 4.2. Selected bond lengths (Å) for **4.1**, **4.2**, and **4.3.**

4.1		**4.2**		**4.3**	
Fe(1)-N(4)	2.007(7)	Fe(1)-N(4)	1.960(2)	Fe(1)-N(5)	1.984(4)
Fe(1)-N(5)	2.010(8)	Fe(1)-N(5)	2.0128(19)	Fe(1)-N(4)	2.011(4)
Fe(1)-N(2)	2.112(6)	Fe(1)-N(2)	2.0867(17)	Fe(1)-N(2)	2.105(3)
Fe(1)-N(3)	2.237(7)	Fe(1)-N(3)	2.2124(18)	Fe(1)-N(1)	2.254(4)
Fe(1)-N(1)	2.249(7)	Fe(1)-N(1)	2.2372(18)	Fe(1)-N(3)	2.258(3)
N(1)-C(2)	1.258(11)	N(1)-C(1)	1.295(3)	N(1)-C(1)	1.277(5)
N(2)-C(3)	1.321(11)	N(2)-C(6)	1.335(3)	N(2)-C(2)	1.335(5)
N(2)-C(7)	1.349(11)	N(2)-C(2)	1.338(3)	N(2)-C(6)	1.350(5)
N(3)-C(8)	1.280(11)	N(3)-C(7)	1.289(3)	N(3)-C(7)	1.275(5)
N(4)-C(34)	1.126(12)	N(4)-C(44)	1.168(3)	N(4)-C(36)	1.156(5)
N(5)-C(35)	1.149(12)	N(5)-C(45)	1.160(3)	N(5)-C(37)	1.156(5)
S(1)-C(34)	1.653(10)	S(1)-C(45)	1.620(3)	S(1)-C(36)	1.615(5)
S(2)-C(35)	1.635(10)	S(2)-C(44)	1.603(3)	S(2)-C(37)	1.629(5)
C(2)-C(3)	1.497(12)	C(1)-C(2)	1.486(3)	C(1)-C(2)	1.477(6)
C(7)-C(8)	1.495(12)	C(6)-C(7)	1.482(3)	C(6)-C(7)	1.482(6)

Table 4.3. Selected bond angles (˚) for compounds **4.1**, **4.2**, and **4.3.**

4.1		**4.2**		**4.3**	
N(4)-Fe(1)-N(2)	150.8(3)	N(4)-Fe(1)-N(5)	118.35(8)	N(5)-Fe(1)-N(4)	102.49(15)
N(5)-Fe(1)-N(2)	106.1(3)	N(4)-Fe(1)-N(2)	148.69(8)	N(5)-Fe(1)-N(2)	142.16(14)
N(4)-Fe(1)-N(3)	104.8(3)	N(5)-Fe(1)-N(2)	92.53(7)	N(4)-Fe(1)-N(2)	115.32(13)
N(5)-Fe(1)-N(3)	102.3(3)	N(4)-Fe(1)-N(3)	104.26(8)	N(5)-Fe(1)-N(1)	105.66(14)
N(2)-Fe(1)-N(3)	73.2(3)	N(5)-Fe(1)-N(3)	98.58(7)	N(4)-Fe(1)-N(1)	95.18(15)
N(4)-Fe(1)-N(1)	98.8(3)	N(2)-Fe(1)-N(3)	73.81(7)	N(2)-Fe(1)-N(1)	73.39(12)
N(5)-Fe(1)-N(1)	101.0(3)	N(4)-Fe(1)-N(1)	96.50(8)	N(5)-Fe(1)-N(3)	99.69(14)
N(2)-Fe(1)-N(1)	71.7(3)	N(5)-Fe(1)-N(1)	95.78(7)	N(4)-Fe(1)-N(3)	100.29(15)
N(3)-Fe(1)-N(1)	142.0(3)	N(2)-Fe(1)-N(1)	73.85(6)	N(2)-Fe(1)-N(3)	73.22(13)
C(2)-N(1)-Fe(1)	117.9(5)	N(3)-Fe(1)-N(1)	145.04(7)	N(1)-Fe(1)-N(3)	146.58(12)
C(10)-N(1)Fe(1)	121.8(5)	C(1)-N(1)-Fe(1)	114.87(14)	C(1)-N(1)-Fe(1)	115.4(3)
C(3)-N(2)-Fe(1)	120.4(6)	C(20)-N(1)-Fe(1)	124.35(13)	C(20)-N(1)-Fe(1)	124.8(2)
C(7)-N(2)-Fe(1)	119.2(5)	C(6)-N(2)-Fe(1)	118.21(14)	C(2)-N(2)-Fe(1)	119.7(3)
C(8)-N(3)-Fe(1)	116.8(6)	C(2)-N(2)-Fe(1)	117.83(14)	C(6)-N(2)-Fe(1)	120.0(3)
C(22)-N(3)-Fe(1)	123.2(5)	C(7)-N(3)-Fe(1)	115.79(14)	C(7)-N(3)-Fe(1)	115.9(3)
C(34)-N(4)-Fe(1)	171.5(8)	C(32)-N(3)-Fe(1)	123.96(14)	C(28)-N(3)-Fe(1)	122.5(2)
C(35)-N(5)-Fe(1)	171.4(7)	C(44)-N(4)-Fe(1)	156.27(19)	C(36)-N(4)-Fe(1)	173.9(4)
C(2)-N(1)-C(10)	120.3(7)	C(45)-N(5)-Fe(1)	170.7(2)	C(37)-N(5)-Fe(1)	168.5(4)
N(4)-C(34)-S(1)	178.7(10)	N(4)-C(44)-S(2)	179.6(2)	N(4)-C(36)-S(1)	178.9(4)
N(5)-C(35)-S(2)	176.9(9)	N(5)-C(45)-S(1)	179.7(3)	N(5)-C(37)-S(2)	179.2(4)

Table 4.4. Summary of Data Collection and Crystallographic Parameters for **4.4** and **4.5**.

Compound	**4.4**	**4.5**
Empirical formula	$C_{37.50}H_{36}Br_2Cl_5FeN_3$	$C_{58}H_{59.50}Br_2Cl_{2.50}FeN_3$
Formula weight	921.61	1102.88
Temperature(K)	200(2)	200(2)
λ (Å)	0.71073	0.71073
Crystal system	Orthorhombic	Monoclinic
Space group	Pbcn	C2/c
a (Å)	19.3043(8)	55.994(7)
b (Å)	17.1881(7)	10.5466(14)
c (Å)	24.3735(9)	19.378(2)
α (deg)	90	90
β (deg)	90	109.047(4)
γ (deg)	90	90
V (Å3)	8087.2(6)	10817(2)
Z	8	8
p (calc) (Mg/m3)	1.514	1.354
m (mm-1)	2.71	1.919
R1a	0.1205	0.1209
wR2b		0.1209

Table 4.5. Selected bond lengths (Å) for **4.4** and **4.5**.

4.4		**4.5**	
Fe(1)-N(2)	2.065(2)	Fe(1)-N(2)	2.071(4)
Fe(1)-N(1)	2.209(2)	Fe(1)-N(1)	2.243(4)
Fe(1)-N(3)	2.215(3)	Fe(1)-N(3)	2.295(4)
Fe(1)-Br(2)	2.3844(5)	Fe(1)-Br(2)	2.3747(10)
Fe(1)-Br(1)	2.4845(5)	Fe(1)-Br(1)	2.4716(11)
N(1)-C(1)	1.287(4)	N(1)-C(1)	1.298(7)
N(2)-C(6)	1.341(4)	N(2)-C(6)	1.333(7)
N(2)-C(2)	1.337(4)	N(2)-C(2)	1.358(7)
N(3)-C(7)	1.284(4)	N(3)-C(7)	1.292(7)
C(1)-C(2)	1.493(4)	C(1)-C(2)	1.483(8)
C(6)-C(7)	1.490(4)	C(6)-C(7)	1.487(8)

Table 4.6. Selected bond angles (˚) for compounds **4.4 and 4.5.**

4.4		**4.5**	
N(2)-Fe(1)-N(1)	73.80(9)	N(2)-Fe(1)-N(1)	74.23(17)
N(2)-Fe(1)-N(3)	74.04(9)	N(2)-Fe(1)-N(3)	72.45(17)
N(1)-Fe(1)-N(3)	143.57(9)	N(1)-Fe(1)-N(3)	142.57(16)
N(2)-Fe(1)-Br(2)	147.47(7)	N(2)-Fe(1)-Br(2)	150.63(14)
N(1)-Fe(1)-Br(2)	98.79(7)	N(1)-Fe(1)-Br(2)	101.52(11)
N(3)-Fe(1)-Br(2)	99.12(7)	N(3)-Fe(1)-Br(2)	99.15(11)
N(2)-Fe(1)-Br(1)	89.83(7)	N(2)-Fe(1)-Br(1)	92.75(13)
N(1)-Fe(1)-Br(1)	98.99(7)	N(1)-Fe(1)-Br(1)	97.04(12)
N(3)-Fe(1)-Br(1)	97.57(7)	N(3)-Fe(1)-Br(1)	101.09(12)
Br(2)-Fe(1)-Br(1)	122.70(2)	Br(2)-Fe(1)-Br(1)	116.60(4)
C(1)-N(1)-Fe(1)	115.95(19)	C(1)-N(1)-Fe(1)	114.2(4)
C(20)-N(1)-Fe(1)	123.10(18)	C(20)-N(1)-Fe(1)	124.9(3)
C(2)-N(2)-Fe(1)	118.66(18)	C(6)-N(2)-Fe(1)	119.8(4)
C(6)-N(2)-Fe(1)	118.22(19)	C(2)-N(2)-Fe(1)	116.8(4)
C(7)-N(3)-Fe(1)	115.5(2)	C(7)-N(3)-Fe(1)	114.6(4)
C(28)-N(3)-Fe(1)	122.92(18)	C(32)-N(3)-Fe(1)	125.7(3)

[4.6] Infra-Red for Iron Complex

Infra-Red spectra were collected using a Cary 630 FT-IR spectrometer.

Table 4.7 : Infra-Red for compounds **4.1**, **4.2**, and **4.3**.

Bond	**4.1**	**4.2**	**4.3**
C=N imine, stretch	1644	1567	1573
-N=C=S, stretch	2047	2046	2046
-N=C=S, stretch	2076	2064	2058

Table 4.8 : Infra-Red for compounds **4.1**, **4.2**, and **4.3**.

Bond	**4.4**	**4.5**
C=N imine, stretch	1582	1566

Chapter 5

Conclusion

This thesis has involved the design of mononuclear cobalt and iron complexes with the goal of understanding and tuning the magnetic features of these compounds and their role as single molecule magnets. A main feature of this effort is to employ the rigid, planar bis(imino)pyridine ligand and the high intrinsic anisotropy ions, to enhance SMM behavior in these systems. This ligand scaffold was used to help to control structural distortion within the coordination geometry of these compounds. We hoped to apply this understanding in the production of new mononuclear SMMs, in a reasonable way. The previous reports have suggested that magnetic anisotropy can be predicted based on the coordination numbers and electronic structures of paramagnetic centres. Recent work from our group and Chang and Long suggests that the SMMs behavior is possible for Co(II) and Fe(II). The approach used in this thesis has led to very unique systems for studying the structural effects on SMM behavior. All previous studies in this field are essentially single examples for SMM behavior, in this work we have a series of not only Co but also Fe complexes.

We employed Co(II) that have a high intrinsic anisotropy among the transition metal ions, and we were successful in synthesizing a number of Co(II)bis(imino)pyridine complexes. The substituents of the bis(imino)pyridine ligand were varied to modify the steric load on both the imine N and C positions. Using X-ray structural analysis, the features of the metal coordination geometry were analyzed. Preliminary magnetic studies were performed on these complexes. These measurements are very interesting and suggest high anisotropy on these complexes. In these complexes the χT value is higher than the expected

theoretical spin-only value of 1.88 cm^3.K/mol for a non-interacting HS Co(II) $S = 3/2$ metal centre ($g = 2$) which is indicative of a high degree of spin-orbit coupling.[51] From this family, compound **3.1** and **3.3** have SMM behaviour but need further analysis.

We attempted very similar chemistry with iron with the goal of synthesizing mononuclear Fe(II) systems. This is interesting in that we can prepare complexes of very similar geometry but that possess one less electron on the metal center. We were able to synthesis and characterize a family of five coordinate Fe(II) compounds. Once again single crystal X-ray analysis provided the means to compare the structural details and their relationship with the imine N and C substituent modifications. We have carried out magnetic studies on these complexes. The first measurements showed that the high anisotropy on these complexes. At room temperature, the χT value is higher than predicted spin-only value of 3 cm^3.K/mol for a non-interacting HS Fe^{II} ion ($S = 2$, $g = 2$), it indicates the high degree of spin-orbit coupling. The Fe compounds still require further magnetic measurements.

This thesis provides a very good basis for our goals of defining structural and electronic influences on single molecule magnetism. The more detailed magnetic measurements that will be carried out in the near future will help lead the way to a better experimental understanding of the interplay of structure and magnetism.